Order Number 1355270

Two-dimensional modeling of flow and sedimentation

Srinivas, Chippada, M.S.

Rice University, 1993

U·M·I
300 N. Zeeb Rd.
Ann Arbor, MI 48106

RICE UNIVERSITY

TWO-DIMENSIONAL MODELING OF FLOW AND SEDIMENTATION

by

Chippada Srinivas

A THESIS SUBMITTED
IN PARTIAL FULFILLMENT OF THE
REQUIREMENTS FOR THE DEGREE

Master of Science

APPROVED, THESIS COMMITTEE:

B. Ramaswamy

Dr. Ramaswamy, Bala, *Chairman*
Assistant Professor
Mechanical Engineering and Materials Science

Mary F. Wheeler

Dr. Wheeler, Mary F.
Professor
Mathematical Sciences

J. E. Akin

Dr. Akin, John E.
Professor
Mechanical Engineering and Materials Science

Houston, Texas

August, 1992

TWO-DIMENSIONAL MODELING OF FLOW AND SEDIMENTATION

Chippada Srinivas

Abstract

A two-dimensional (vertical) flow model is developed to simulate open channel flow. The governing equations are solved without any depth averaging. Free surface movement is handled with the help of Arbitrary Lagrangian Eulerian Method. $k-\epsilon$ closure is employed to determine the turbulent eddy viscosity. Spatial discretization is done using linear 3-noded triangular elements. Galerkin method of weighted residuals is used to obtain weak form formulation. Navier-Stokes equations are solved by marching in time using Fractional Step Scheme. Continuity equation is replaced with a pressure Poisson equation. Supercritical flow and hydraulic jump are simulated to validate the flow code.

Suspended sediment transport is modeled using an advection-diffusion transport equation for sediment concentration. Bed load transport is determined with the help of empirical correlations. The boundary condition at the bed is specified as a reference concentration. Sample problem involving bed erosion and deposition is solved.

Acknowledgments

I sincerely thank my thesis advisor Dr. Bala Ramaswamy, for his guidance, advice, and encouragement during this research. I would also like to thank Dr. John E. Akin, and Dr. Mary F. Wheeler for serving on the dissertation committee.

The financial support by the Rice University, Texaco Inc. and National Science Foundation is greatly appreciated. This research wouldn't have been possible without the excellent computational resources offered by the Department of Mechanical Engineering and Material Science and CRAY Research Inc. I learned a lot from Dr. T. C. Jue, Mr. Lawrence Cowsar and Dr. Dan Tetzlaff with whom I had many fruitful discussions on the subject of this research.

Nomenclature

Symbols	Explanation
a	reference height above the bed
A	cross-sectional area of the channel
b	bed height above a datum
B	width of the free surface
c	suspended sediment concentration
c_a	reference suspended sediment concentration at height a above the bed
C	constant in Chézy's equation for uniform flow
D	diameter of the sediment particle
D_H	hydraulic depth of an open channel
D_*	non-dimensional particle parameter
g	gravitational acceleration
h	height of the free surface
k	turbulent kinetic energy
M	mass matrix
M_D	lumped mass matrix
M_C	consistent mass matrix
n	Manning's n occuring in the uniform flow formula
p	pressure
R	hydraulic radius

s	specific density of sediment
$S-b$	total bed load transport across a cross-section
$S-s$	total suspended load transport across a cross-section
S, S_0	slope of the channel bed in radians
S_f	friction slope or resistance at the bed
t	time
T	non-dimensional transport parameter
Δt	time increment
u	velocity component in the x-direction
u_*	shear velocity at the bed
$u_{*,cr}$	critical shear velocity for threshold motion
U	mean velocity in the x-direction
v	velocity component in the y-direction
w	velocity component in the z-direction
w_s	suspended sediment particle fall velocity
(x, y, z)	Cartesian coordinate
Z	non-dimensional suspension parameter
x_i	Cartesian coordinate in i-th direction
$\Delta x, \Delta y$	spatial increment in x and y directions

Greek Letters

$\alpha_L \& \alpha_R$	lumping parameters on the LHS and RHS respectively
ϵ	turbulent dissipation rate
κ	von Karman const.
μ	coefficient of viscosity
ν	coefficient of kinematic viscosity

ν_t	turbulent kinematic viscosity
Ω	bounded domain of R^d
ϕ	porosity of the bed
Φ_α	shape function
ρ	fluid density
σ	surface tension
σ_{ij}	stress tensor
τ	tangential direction
τ_c	critical shear stress for threshold motion given by Shields
$\bar{\tau}$	time domain

Subscripts

i, j, k	directions of Cartesian coordinate
t	derivative with time
x	derivative w. r. t. x
α, β, γ	nodal number
$,i$	partial derivative w. r. t. x_i

Superscripts

n	n-th time steps
$*$	refers to dimensional value
$\tilde{}$	intermediate value

Nondimensional Numbers

Fr	Froude number, $Fr = \frac{U}{\sqrt{gL}}$
Re	Reynolds number, $Re = \frac{LU}{\nu}$
We	Weber number, $We = \frac{U}{\sqrt{\frac{\sigma}{\rho L}}}$

Note: The symbols defined aboved are subject to alteration on occasion.

Table of Contents

List of Figures

Chapter 1

INTRODUCTION

Open channel flow and sediment transport have applications in many fields of engineering. Hydraulic engineers need thorough understanding of open channel flow for designing efficient channels, spillways, dams, reservoirs etc. Sedimentation plays no small role in topographical evolution of earth through its influence on the evolution of river-beds, estuaries, coast-lines, and stratification of the earth's surface. Numerous problems such as soil erosion, irrigation, flood control, navigation, hydraulic structure safety, environmental quality, etc. are closely related to sedimentation processes. The knowledge of sedimentation is also useful in predicting the permeability and porosity distributions which is useful in oil and gas exploration and production, and remediation of contaminated aquifiers.

Simulation of open channel flow is not easy. The physical nature of free surface flow is fairly well understood and the governing mathematical equations are the well known Navier-Stokes equations. However the difficulty arises in solving these equations. Flow in most cases is turbulent and there are widely varying length scales. The channel geometries are complex and extend over hundreds of miles making it prohibitively expensive to numerically discretize the whole physical domain.

Modeling sedimentation is even more complicated since even the physical laws governing them are not known. Added to this is the fact that sediment transport has some elements of stochastics in it. Close to the bed where the concentration of sediment is considerable the normal flow equations are no longer valid. The sediment sizes and shapes vary a lot from fine silt to boulder-sized particles. Thus to obtain one

set of physical laws which would be applicable in all of these widely varying situations is very difficult. Progress has also been hampered by the problem of measuring sediment transport.

In this research an effort is made to overcome some of the above mentioned difficulties. Our strategy towards solving the open-channel flow is to make no simplifications such as depth or cross-section averaging as has been done in the past, but to solve the complete 2-D Reynolds averaged Navier Stokes equations. Use would be made of the powerful numerical algorithms which have been developed in the past few years. Further, with the advent of massively parallel computing machines the day when Navier-Stokes equations can be solved for real life large scale problems is not far. Since our flow model would not have some of the constraints which the previous models had we would be able to determine important parameters such as bed-shear stress more accurately and this would help in better modeling and understanding of sediment transport. Our code can also be used to test some of the sediment transport models being proposed and hence would help in determining better sedimentation equations.

In the next few chapters various aspects of open channel flow are discussed and some sample problems are solved to test the accuracy and robustness of the flow code. Then this flow code is coupled with a sediment transport model to simulate sedimentation and bed erosion. Finally we summarize our efforts and establish future research directions and goals.

Chapter 2

OPEN CHANNEL FLOW CHARACTERISTICS

In this chapter we discuss open-channel flow and some of its important features. Only issues important from the point of view of numerical modeling are discussed. For a more detailed description the excellent texts on this subject by Chow(1959) and Henderson(1966) are good references.

An open channel is a conduit in which water flows with a free surface. Classified according to its origin a channel may be either natural or artificial. Although there are many similarities between open-channel flow and pipe flow one important difference between the two is the presence of free surface in open-channel flow. Open-channel flow is more difficult to study than pipe flow and some of the reasons are [Chow,1959]:

- position of the free surface likely to change with time and space.
- depth of the flow, the discharge, and the slope of the channel bottom and of the free surface are interdependent.
- reliable experimental data more difficult to obtain.
- physical conditions of open channels vary much more widely than pipe flow, e.g., cross-section can be any shape, surface roughness varies more widely than in pipe flow.

The state or behaviour of open-channel flow is governed basically by the effects of viscosity, surface tension and gravity relative to the inertial forces of the flow.

2.1 Effect of Viscosity

The effect of viscosity relative to inertia can be represented by the Reynolds number, defined as

$$Re = \frac{UL}{\nu} \tag{2.1}$$

where U is the characteristic velocity, L is the characteristic length and ν is the kinematic viscosity of water. It is well known that below a certain critical value of the Reynolds number the flow will be laminar in nature, while above this value, flow would be turbulent. For pipe flow this critical Reynolds number for transition to turbulence has been found to be around 2,000. But unlike in pipe flow, in an open channel a large part of the total thickness continues to be occupied by the relatively nonturbulent "laminar sublayer," even at large flow rates ($Re \gg Re_{crit}$). Hence, the transition from laminar to turbulent flow cannot be expected to be so sharply marked as in the case of pipe flow. Nevertheless, it is of value to subdivide film flow into laminar and turbulent regimes depending on whether ($Re <> Re_{crit}$). For practical purposes, the transitional range of Re for open-channel flow may be assumed to be 500 to 2000 [Chow,1959]. In open-channel flow the characteristic length is made equal to the hydraulic depth D_H, which is defined as the cross-sectional area of the water normal to the direction of flow in the channel divided by the width of the free surface.

Laminar flow occurs very rarely in open channels. The fact that the surface of a stream appears smooth and glassy to an observer is by no means an indication that the flow is laminar; most probably, it indicates that the surface velocity is lower than that required for capillary waves to form. Laminar open-channel flow is known to exist, however, usually where thin sheets of water flow over ground or where it is created deliberately in model testing channels.

2.2 Effect of Gravity

The effect of gravity upon the state of flow is represented by the ratio of inertial forces to gravity forces. This ratio is given by the Froude number, defined as

$$Fr = \frac{U}{\sqrt{gL}} \tag{2.2}$$

where U is the mean velocity of flow, g is the acceleration due to gravity, and L is a characteristic length. There are three states of flow depending on the value of Fr:

- $Fr = 1$, the flow is said to be in a critical state.
- $Fr < 1$, the flow is said to be in a subcritical state. In this state the role played by gravity forces is more pronounced; so the flow has a low velocity and is often described as tranquil and streaming.
- $Fr > 1$, the flow is said to be in a supercritical state. In this state the inertial forces become dominant; so the flow has a high velocity and is usually described as rapid, shooting, and torrential.

In the mechanics of water waves, the critical velocity $\sqrt{gL}$ is identified as the celerity of the small gravity waves that occur in shallow water in channels as a result of any momentary change in the local depth of the water. Such a change may be developed by disturbances or obstacles in the channel that cause a displacement of water above and below the mean water surface level and thus create waves that exert a weight or gravity force. It should be noted that a gravity wave can be propagated upstream in water of subcritical flow, since the celerity is greater than the velocity of flow. Therefore, the possibility or impossibility of propagating a gravity wave upstream can be used as a criterion for distinguishing between subcritical and supercritical flow.

2.3 Effect of Surface Tension

The effect of surface tension on the flow can be expressed by the ratio of inertial forces to surface tension forces given by,

$$We = \frac{V}{\sqrt{\frac{\sigma}{\rho L}}} \tag{2.3}$$

where σ is surface tension and ρ is density of the fluid. Analogous to Froude number, Weber number(We) also represents the ratio of mean fluid velocity to the celerity of a capillary wave in shallow channels. The surface tension of water may affect the behaviour of flow under certain circumstances, but it does not play a significant role in most open-channel problems encountered in engineering.

2.4 Rapid Variations in Flow

Change of the state of flow from subcritical to supercritical or vice versa occur frequently in open channels. Such change is manifested in a corresponding change in the depth of flow. If the change takes place rapidly over a relatively short distance the flow is said to be rapidly varied. Rapidly varied flow has very pronounced curvature of stream lines and is usually in a high state of turbulence resulting in separation zones, eddies and rollers. The hydraulic drop and hydraulic jump are two types of local phenomena and are described below.

Hydraulic Drop: A rapid change from a high stage to a low stage (i.e., from subcritical to supercritical) will result in a steep depression in the water surface. Such a phenomenon is generally caused by an abrupt change in the channel slope or cross section and is known as hydraulic drop.

Hydraulic Jump: When the rapid change in the depth of flow is from a low stage to a high stage (i.e., from supercritical to subcritical), the result is usually an abrupt rise of water surface. This local phenomenon is known as the hydraulic jump. The hydraulic jump involves a relatively large amount of energy loss through turbulent dissipation.

Consequently, the energy content in the flow after the jump is appreciably less than that before the jump.

2.5 Flow Modeling Aspects

In the preceding sections some of the important features of open channel flow have been discussed. The flow model to be developed should have the capability to simulate these features. For clarity some of the open-channel features important from numerical modeling point of view are restated below:

1. Free surface could vary with time and space.
2. In most instances flow is turbulent.
3. The channel bottom roughness varies a lot and has a significant effect on the flow.
4. The flow could change rapidly as in the case of a hydraulic jump or hydraulic drop resulting in large gradients in flow height and velocities(similar to shock waves in compressible flow).
5. The channel geometry in general is very irregular and complex. Also the channels could be curving and meandering giving rise to secondary currents.
6. In natural river bodies like estuaries and lakes, periodic phenomena such as tidal currents and waves are of significance.
7. Disturbances propagate as gravity waves on the free surface.
8. Surface tension is not very significant in most open-channel flows and can be neglected.

9. Sediment transport could lead to bed deformation and formation of bed form features such as ripples and dunes. Thus not only the free surface but the bed also changes with time and affects the flow.

Chapter 3

GOVERNING EQUATIONS FOR OPEN CHANNEL FLOW

3.1 Unsteady Open Channel Flow Equations

The governing equations for the fluid flow are the well known incompressible Navier-Stokes equations and the continuity equation. The equations in cartesian co-ordinates for a typical open-channel as shown in Fig.3.1 are given by [Lai,1986]:

$$\frac{\partial u}{\partial x} + \frac{\partial v}{\partial y} + \frac{\partial w}{\partial z} = 0 \tag{3.1}$$

$$\frac{\partial u}{\partial t} + u\frac{\partial u}{\partial x} + v\frac{\partial u}{\partial y} + w\frac{\partial u}{\partial z} = -\frac{1}{\rho}\frac{\partial p}{\partial x} + \nu \bigtriangledown^2 u \tag{3.2}$$

$$\frac{\partial v}{\partial t} + u\frac{\partial v}{\partial x} + v\frac{\partial v}{\partial y} + w\frac{\partial v}{\partial z} = -\frac{1}{\rho}\frac{\partial p}{\partial y} + \nu \bigtriangledown^2 v \tag{3.3}$$

$$\frac{\partial w}{\partial t} + u\frac{\partial w}{\partial x} + v\frac{\partial w}{\partial y} + w\frac{\partial w}{\partial z} = -g - \frac{1}{\rho}\frac{\partial p}{\partial z} + \nu \bigtriangledown^2 w \tag{3.4}$$

u,v, and w are the x,y,z components of flow velocity ; p,ν,ρ, and t stand for fluid pressure, kinematic viscosity, fluid density, and time: and the symbol $\bigtriangledown^2$ signifies the Laplace operator

$$\bigtriangledown^2 = \frac{\partial^2}{\partial x^2} + \frac{\partial^2}{\partial y^2} + \frac{\partial^2}{\partial z^2} \tag{3.5}$$

The effect of earth's rotation which gives rise to Coriolis force has been neglected in the above mathematical system. Coriolis force is however important if the channels are very wide and should be accounted for in such cases.

3.2 Uniform Flow Formulas

Flow is said to be uniform if the velocity distribution across the channel cross section is constant along the channel. This is attained when the boundary layer is fully

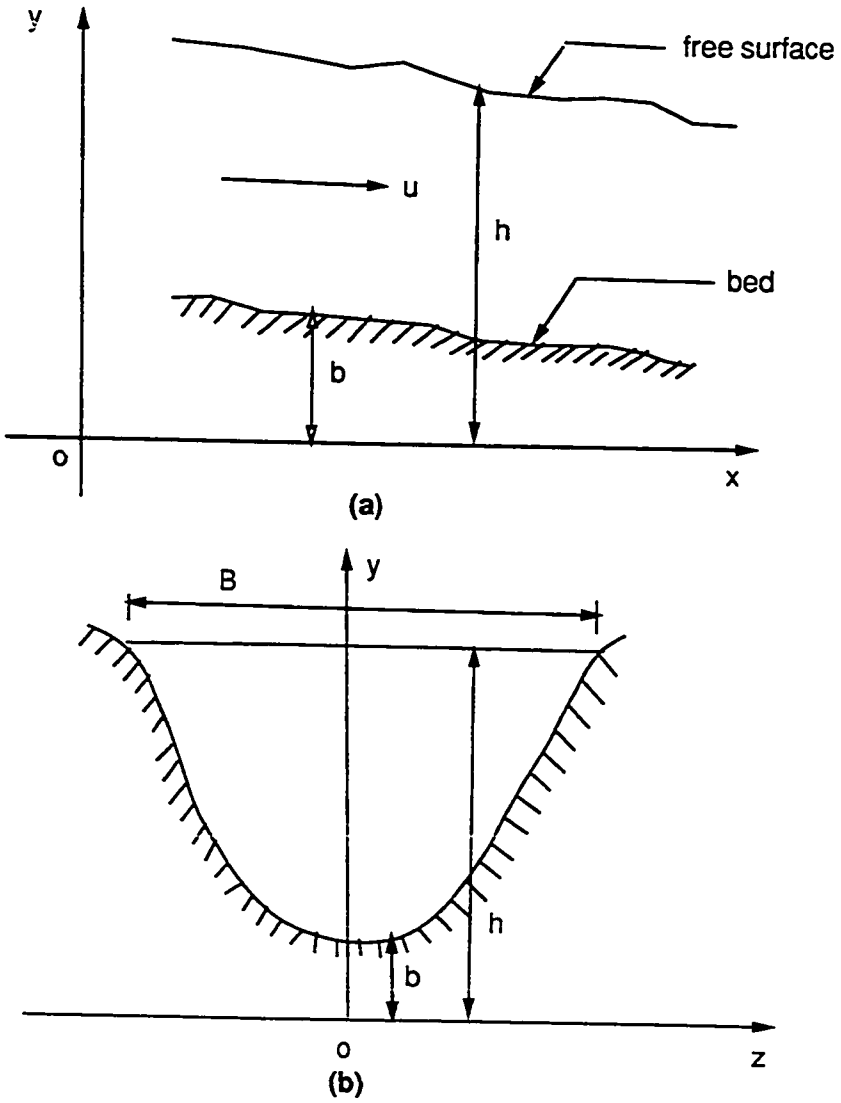

Figure 3.1: Typical open-channel geometry: (a)profile and (b) cross section.

developed and reaches the free surface. However, uniform flow cannot occur at high velocities as the flow becomes unstable and if the velocity is further increased entrainment of air occurs. The best known and the most widely used uniform flow formulas are Chézy and Manning formulas. The Chézy formula is expressed as

$$U = C\sqrt{RS} \tag{3.6}$$

and the Manning formula is expressed as

$$U = \frac{\lambda}{n} R^{2/3} S^{1/2} \tag{3.7}$$

where U is the mean velocity, R is the hydraulic radius and S is the slope of the channel, C is the factor of resistance also called Chézy's C and n is the roughness coefficient also called Manning's n. In metric and inch-pound systems, λ assumes values of 1 and 1.486, respectively. C and n are dependent on various factors such as channel roughness, geometry, discharge, flow depth, viscosity etc.

3.3 Shallow Water Equations

The momentum and continuity equations are integrated in the vertical direction to remove the dependency on the vertical coordinate. Thus 3-D equations are converted into 2-D. Denoting $\bar{u}$ and $\bar{w}$ as the mean values of u and w over the vertical,

$$\bar{u} = \frac{1}{h-b} \int_b^h u \, dz \tag{3.8}$$

$$\bar{w} = \frac{1}{h-b} \int_b^h w \, dz \tag{3.9}$$

The continuity equation for two-dimensional (x-z plane) shallow water flow is given by [Lai, 1986]:

$$\frac{\partial h}{\partial t} + \frac{\partial}{\partial x}(h\bar{u}) + \frac{\partial}{\partial z}(h\bar{w}) = 0 \tag{3.10}$$

In the derivation of above equation lateral inflow or outflow due to rain fall, evaporation or seepage has not been considered.

In a nearly horizontal flow, the vertical acceleration of a fluid particle is very small compared with the acceleration of gravity g and may be neglected. It is further

assumed that shear stress due to the vertical velocity component is also negligible. Thus the z-momentum equation reduces to

$$0 = -\rho g - \frac{\partial p}{\partial z} \tag{3.11}$$

Integrating and, assuming the atmospheric pressure p_a to be zero we obtain,

$$p = \rho g\,(h - y) \tag{3.12}$$

Above equation tells us that pressure in the vertical direction is hydrostatic, which is found to be a reasonable approximation if the slope of the channel is not too large [Henderson, 1966]. Thus,

$$\frac{\partial p}{\partial x} = \rho g \frac{\partial h}{\partial x} \tag{3.13}$$

$$\frac{\partial p}{\partial z} = \rho g \frac{\partial h}{\partial z} \tag{3.14}$$

Integrating the x and y momentum equations in the vertical directions we obtain

$$\frac{\partial}{\partial t}(\bar{u}h) + \frac{\partial}{\partial x}\left[\beta_x \bar{u}^2 (h-b)\right] + \frac{\partial}{\partial z}\left[\beta_{xz}\bar{u}\bar{v}(h-b)\right] = -g\frac{\partial h}{\partial x}(h-b) - g(h-b)S_{fx} \tag{3.15}$$

$$\frac{\partial}{\partial t}(\bar{w}h) + \frac{\partial}{\partial x}\left[\beta_{xz}\bar{u}\bar{w}(h-b)\right] + \frac{\partial}{\partial z}\left[\beta_z \bar{w}^2 (h-b)\right] = -g\frac{\partial h}{\partial z}(h-b) - g(h-b)S_{fz} \tag{3.16}$$

where

$$\beta_x \bar{u}^2 = \frac{1}{h-b}\int_b^h u^2\,dy \tag{3.17}$$

$$\beta_{xz}\bar{u}\bar{w} = \frac{1}{h-b}\int_h^b uw\,dy \tag{3.18}$$

$$\beta_z \bar{w}^2 = \frac{1}{h-b}\int_b^h w^2\,dy \tag{3.19}$$

S_{fx} and S_{fz} are the shear stress at the bed in x and z directions, respectively and are determined using uniform flow formulas such as Manning's formula or Chézy's equation. β_x, β_z and β_{xz} are called momentum correction factors and are often assumed to be unity.

3.4 Saint-Venant Equations

If the above derived 2-D shallow water equations are further integrated in the z direction we obtain the famous Saint-Venant equations. These are nothing but the

cross-section averaged Navier-Stokes and continuity equations. Most of the numerical study in open-channels is done using these 1-D Saint-Venant equations. 2-D shallow water equations are used only when the open-channels are very wide as in the case of large estuaries or lakes.

$$B\frac{\partial h}{\partial t} + \frac{\partial}{\partial x}(UA) = 0 \tag{3.20}$$

$$\frac{\partial}{\partial t}(UA) + \frac{\partial}{\partial x}(U^2A) + gA\frac{\partial h}{\partial x} + gA(S_f - S_0) = 0 \tag{3.21}$$

where A is the cross-sectional area of the channel, B is the width of the free surface, U is the average velocity across the cross-section, S_f is the friction slope determined from any of the empirical formulas and S_0 is the slope of the channel bed in x-direction. There have been a number of assumptions and approximations in deriving these averaged equations which are explained in great detail in Lai(1986).

3.5 Previous 3-D Unsteady Flow Models

To date not much 3-D modeling has been done in hydrodynamics. However, with the rapid progress made in the computer hardware and algorithms, in recent years some 3-D modeling work has been done. However these are not complete 3-D models but contain some approximations to make solution on the computers feasible. Some of the ideas incorporated in these 3-D models are listed below:

1. Multi-layered type models have been developed in which the the flow is divided into many layers and 2-D shallow water equations are assumed to be valid in each layer. This gives a better representation of the shear stresses at each layer [Su, 1986].

2. Higher degree polynomial bases functions are used to describe the vertical structure. For instance, the vertical variation of the horizontal velocities could be taken to be hermite cubic and this can even handle recirculation regions [McCarty(1986)].

3. Rigid-lid models are some times used if the free surface doesn't vary much from a mean flow height. This is done to overcome the stringent restriction imposed by surface gravity waves on the maximum time step allowed in time marching schemes. In this case the gravity waves no longer exist as the free surface cannot move[Sheng, 1978].

4. Procedures have been developed which divide the computations into a external-mode calculation and an internal mode calculation. In the external mode calculations free surface height and average velocities are computed from the depth averaged equations. Even though the gravity waves limit the time step severely the calculations are not too expensive since they are only 2-D calculations. Once in a few time steps full 3-D calculations are done and this is called internal mode step. This step gives us more accurate shear stresses since it is a full 3-D model and these shear stresses are used in the external mode step [Sheng, 1978].

3.6 2-D Flow Model Definition

From the preceding paragraphs it can be concluded that flow in an open-channel is governed by the incompressible 3-D Navier Stokes equations. But, since it is difficult to solve them numerically or otherwise depth averaged and cross-section averaged models are being used by the hydraulic engineers. Only recently researchers have started doing 3-D or pseudo 3-D modeling. It must be recognized that accurate predictions of velocities and shear stresses are necessary to model sediment transport. Thus our efforts are going to be towards solving complete 3-D Navier Stokes equations. But, as a first step 2-D Navier Stokes equations are solved to better understand the various concepts and difficulties involved in the modeling of open-channel flow and sedimentation. Use of 2-D equations essentially mean that the variables are assumed to be invariant in the z-direction (width) and there are no velocities in this direction.

The physical domain is illustrated in the Fig.3.2. The x-axis is taken to be along the bed. Thus if the channel is inclined then the body force (gravity) has components in both x and y directions. The 2-D flow equations are:

$$\frac{\partial u}{\partial t} + u\frac{\partial u}{\partial x} + v\frac{\partial u}{\partial y} = gsin\theta - \frac{1}{\rho}\frac{\partial p}{\partial x} + \frac{\partial}{\partial x}\nu\frac{\partial u}{\partial x} + \frac{\partial}{\partial y}\nu\frac{\partial u}{\partial y} \tag{3.22}$$

$$\frac{\partial v}{\partial t} + u\frac{\partial v}{\partial x} + v\frac{\partial v}{\partial y} = -gcos\theta - \frac{1}{\rho}\frac{\partial p}{\partial y} + \frac{\partial}{\partial x}\nu\frac{\partial v}{\partial x} + \frac{\partial}{\partial y}\nu\frac{\partial v}{\partial y} \tag{3.23}$$

$$\frac{\partial u}{\partial x} + \frac{\partial v}{\partial y} = 0 \tag{3.24}$$

An additional equation is needed to determine the free surface height. This is obtained from the kinematic equation for the free surface:

$$\frac{\partial h}{\partial t} + u\frac{\partial h}{\partial x} = v \tag{3.25}$$

At the channel bed no slip and impermeable boundary conditions give us

$$u = 0, \text{ and } v = 0 \text{ at the wall.} \tag{3.26}$$

At the free surface the normal stress equals the atmospheric pressure after neglecting the surface tension.

$$p - 2\nu\frac{\partial u_n}{\partial n} = p_a \tag{3.27}$$

Usually due to the high Reynolds number the viscous stresses at the free surface can be neglected and taking $p_a = 0$ we obtain,

$$p = 0, \quad \text{on the free surface.} \tag{3.28}$$

The tangential stress should equal the stresses due to wind but they are generally neglected. Therefore,

$$\nu\left(\frac{\partial u_\tau}{\partial n} + \frac{\partial u_n}{\partial \tau}\right) = 0 \quad \text{on the free surface.} \tag{3.29}$$

Eqs.3.28 & 3.29 together represent the boundary conditions on the free surface. At the inlet the velocities are imposed as dirichlet boundary conditions.

$$u = U_{in} \text{ and } v = V_{in} \text{ at the inlet.} \tag{3.30}$$

At the exit normally fully developed velocity profile boundary conditions are imposed.

$$\frac{\partial u}{\partial x} = 0 \text{ and } v = 0 \text{ at the exit.} \tag{3.31}$$

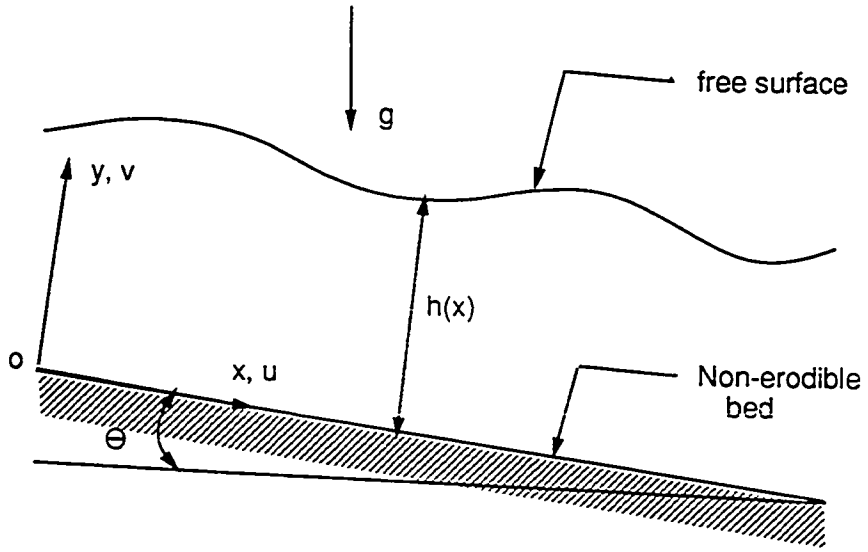

Figure 3.2: Two dimensional physical domain

At the inlet the free surface height is specified.

$$h = H_{in} \text{ at the inlet} \tag{3.32}$$

and at the exit we may or may not specify the free surface height, i.e., it depends on the problem.

Rest of this work concerns itself with solving the four equations 3.22,3.23,3.24 and 3.25 for u,v,p and h with appropriate boundary conditions as explained above. However the physical modeling is not complete yet. In the next chapter we discuss turbulence and the inclusion of two more dependent variables, namely, the turbulent kinetic energy (k) and the turbulent dissipation rate (ϵ) in our model.

Chapter 4

TURBULENCE

4.1 Reynolds Averaged Equations

As already mentioned, open channel flow as it occurs in nature is almost always turbulent. Hinze(1975) defines turbulence as "Turbulent fluid motion is an irregular condition of flow in which the various quantities show a random variation with time and space coordinates, so that statistically distinct average values can be discerned." It is believed that the solution of time-dependent 3-D Navier-Stokes equations can describe turbulent flows completely. The reason why these equations cannot be solved as they are is that the length scales occuring in turbulence are very small and would require a very small grid spacing and consequently small time step to numerically resolve these scales. This is beyond the reach of the present day computers. The main thrust of present day research in turbulent flows is through the time-averaged Navier-Stokes equations. These equations are also referred to as the Reynolds equations of motion or the Reynolds averaged equations.

The Reynolds equations are derived by decomposing the dependent variables in the conservation equations into time mean (obtained over an appropriate time interval) and fluctuating components and then time averaging the entire equation.

$$u = \bar{u} + u', \quad v = \bar{v} + v', \quad w = \bar{w} + w', \quad p = \bar{p} + p'$$

The Reynolds averaged continuity and momentum equations are:

$$\frac{\partial \bar{u}_j}{\partial x_j} = 0 \tag{4.1}$$

$$\frac{\partial \bar{u}_i}{\partial t} + \frac{\partial}{\partial x_j}(\bar{u}_i \bar{u}_j) = -\frac{\partial \bar{p}}{\partial x_i} + \frac{\partial}{\partial x_j}(\nu \frac{\partial \bar{u}_i}{\partial x_j} - \overline{u_i' u_j'}) \tag{4.2}$$

Due to the nonlinear advection terms the fluctuating components donot disappear with Reynolds averaging but reappear as $\overline{u_i' u_j'}$ which are called the apparent stresses or Reynolds stresses. These new quantities (six of them) are to be determined from the mean flow field and presents us with the classic closure problem. These terms are modeled using physical and dimensional arguments and the unknown coefficients are tuned using experimental data.

Some of the most commonly used models for turbulent simulation are discussed in the next few sections.

4.2 Zero equation model

Prandtl's mixing length hypothesis which is the first turbulence model ever proposed, is still among the most widely used models. It employs the eddy viscosity concept which relates the turbulent transport terms to the local gradient of mean flow quantities. For example, for thin shear layers

$$-\overline{uv} = \nu_t \frac{\partial \bar{u}}{\partial y} \tag{4.3}$$

where ν_t = eddy viscosity. The Prandtl's mixing length hypothesis calculates the distribution of eddy viscosity by relating it to the mean velocity gradient:

$$\nu_t = C_\mu l_m^2 \mid \frac{\partial \bar{u}}{\partial y} \mid \tag{4.4}$$

This relation involves a single unknown parameter, the mixing length l_m whose distribution over the flow field has to be prescribed with the aid of empirical information. The mixing length model has been used for free shear layers and wall boundary layers. The main drawback of this model is the evaluation of l_m for different flows. The incorporation of the effects of curvature, buoyancy or rotation in the model is entirely empirical. The transport and history effects of turbulence are not accounted in the mixing length model. The more generally applicable models to be described below account for these effects by introducing transport equations for turbulent quantities.

4.3 One Equation Models

The one equation model requires the solution of an equation for the turbulent kinetic energy, k and, as a result, allows for its transport. The transport equation for turbulent kinetic energy can be derived from the Navier-Stokes equations.

$$k = \frac{1}{2}\overline{u_i' u_i'} \tag{4.5}$$

The eddy viscosity is modeled by $\nu_t = C_\mu k^{1/2} l$. The length scale l is specified algebraically and hence is flow dependent. It is difficult to incorporate the length scale empirically for complex flows with separation, streamline curvature or rotation. One equation model is not very popular since it performs only marginally better than the zero equation model.

4.4 Two equation Models

This class of models is the one widely used in the present day engineering calculations. In attempts to eliminate the need for specifying the turbulence length scale as a function of position throughout the flow, a second differential equation which in effect gives l has been used. Some of the two equation models proposed are $k - kl$, $k - \omega$, and $k - \epsilon$, where l is the length scale of turbulence, ω is the time average square of the vorticity fluctuations, and ϵ is the dissipation rate of turbulent kinetic energy.

$$\epsilon = \nu \overline{\frac{\partial u_i'}{\partial x_k} \frac{\partial u_l'}{\partial x_k}} \tag{4.6}$$

It is possible to transform $k - \epsilon$ into $k - \omega$ and vice versa. However, the $k - \epsilon$ model has become the most popular because of the practical advantage that the ϵ-equation requires no extra terms near the walls. Also, ϵ itself appears in the k-equation and the ϵ-equation requires no secondary source term.

4.5 Reynolds Stress Models

The main limitations of the two equation models are the assumption of isotropic eddy viscosity and the need to model buoyancy, rotation and curvature effects separately. In the models discussed so far the local state of turbulence is assumed to be characterized by one velocity scale $\sqrt{k}$. In actual flows, the scales may develop quite differently. In order to account for the different development of the individual stresses, transport equations for $\overline{u_i u_j}$ have been introduced. In this model one needs to solve the equation for the turbulence energy dissipation rate ϵ, in addition to those for $\overline{u_i u_j}$ for the length scale. A particular advantage of the Reynolds stress model is that terms accounting for buoyancy, rotation and other effects are in principle introduced automatically. Because of the complexity and the large amount of computational effort required, the model has not been used much [Nallasamy, 1987].

4.6 Algebraic Stress Model

In Reynolds stress models, there are differential transport equations for each component of $\overline{u_i u_j}$ in addition to the ϵ equation. To reduce the computational effort, Rodi(1984) proposed an algebraic relation for calculating the Reynolds stresses. The convection and diffusion terms in the transport of $\overline{u_i u_j}$ are replaced by model approximations, reducing the equations to algebraic equations. The algebraic expressions together with k and ϵ equations form an extended $k - \epsilon$ model. Algebraic stress models can simulate many of the flow phenomena that were described successfully by stress-equation models without being too computationally expensive..

4.7 Large Eddy Simulation (LES)

This method calculates the large-scale structures of the turbulence explicitly, while modeling the small ones. It is three-dimensional and time dependent, and provides

considerable detail about a flow. This makes it a valuable tool for investigating both the physics of turbulence and the models used to represent it. Its application is currently limited to simple flows and relatively low Reynolds numbers. It is too expensive for direct engineering use at the present time, but may see limited use in engineering design as the cost of supercomputers comes down and their number increases [Ferziger,1985].

4.8 Full Turbulence Simulation

In this approach, one solves the unaveraged time dependent Navier-Stokes equations for a turbulent flow numerically. The set of flows which can be treated in this way is small, but its accuracy makes it a complement to laboratory experiments for investigation of both physics and turbulence models. It is also ideal for investigating phenomena associated with the small scales of turbulence, especially subgrid scale models for large-eddy simulation.

4.9 Selection of Turbulence Model : $k-\epsilon$ Turbulence Model Chosen

In summary it could be said that the more number of transport equations to calculate the Reynolds stresses the more accurate is our representation but at the same time more expensive too. Thus our selection is essentially a compromise between accuracy and cost effectiveness. According to the ASCE Task Committee(1988) appointed to look into the use of turbulence models for simulation of hydraulic flows, $k-\epsilon$ model is the one being most widely used. The $k-\epsilon$ model predicts the flow fairly accurately. It has the additional advantage (over mixing length models) that it can simulate recirculating flows also. Thus $k-\epsilon$ model has been chosen by us to model turbulence.

The $k-\epsilon$ model employs the eddy viscosity and relates it to k and ϵ. In addition to the momentum and continuity equations there are two additional transport equation to be solved, one for turbulent kinetic energy (k) and another for dissipation rate of turbulence kinetic energy (ϵ). The most widely used $k-\epsilon$ model is the one proposed by Launder(1974).

$$\frac{Dk}{Dt} = \frac{1}{\rho}\frac{\partial}{\partial x_k}\left[\frac{\nu_t}{\sigma_k}\frac{\partial k}{\partial x_k}\right] + \nu_t\left(\frac{\partial U_i}{\partial x_k} + \frac{\partial U_k}{\partial x_i}\right)\frac{\partial U_i}{\partial x_k} - \epsilon \tag{4.7}$$

$$\frac{D\epsilon}{Dt} = \frac{1}{\rho}\frac{\partial}{\partial x_k}\left[\frac{\nu_t}{\sigma_\epsilon}\frac{\partial \epsilon}{\partial x_k}\right] + C_1\nu_t\frac{\epsilon}{k}\left(\frac{\partial U_i}{\partial x_k} + \frac{\partial U_k}{\partial x_i}\right)\frac{\partial U_i}{\partial x_k} - C_2\frac{\epsilon^2}{k} \tag{4.8}$$

$$\nu_t = C_\mu k^2/\epsilon \tag{4.9}$$

The constants in these equations are[Launder, 1974]:

$$C_\mu = 0.09, \quad C_1 = 1.44, \quad C_2 = 1.92, \quad \sigma_k = 1.0, \quad \sigma_\epsilon = 1.3$$

The coefficients are constants in the sense that they are not changed in any calculation. However, these constants need to be changed in order to accomodate the effects such as curvature, low Reynolds number, near wall, etc. Dropping the bars on top of the variables, since no ambiguity would result the mathematical system to be solved is:

$$\frac{\partial u}{\partial x} + \frac{\partial v}{\partial y} = 0 \tag{4.10}$$

$$\frac{\partial u}{\partial t} + u\frac{\partial u}{\partial x} + v\frac{\partial u}{\partial y} = gsin\theta - \frac{1}{\rho}\frac{\partial p}{\partial x} + \frac{\partial}{\partial x}(\nu+\nu_t)\frac{\partial u}{\partial x} + \frac{\partial}{\partial y}(\nu+\nu_t)\frac{\partial u}{\partial y} \tag{4.11}$$

$$\frac{\partial v}{\partial t} + u\frac{\partial v}{\partial x} + v\frac{\partial v}{\partial y} = -gcos\theta - \frac{1}{\rho}\frac{\partial p}{\partial y} + \frac{\partial}{\partial x}(\nu+\nu_t)\frac{\partial v}{\partial x} + \frac{\partial}{\partial y}(\nu+\nu_t)\frac{\partial v}{\partial y} \tag{4.12}$$

$$\frac{\partial h}{\partial t} + u\frac{\partial h}{\partial x} = v \tag{4.13}$$

$$\frac{Dk}{Dt} = \frac{1}{\rho}\frac{\partial}{\partial x_k}\left[\frac{\nu_t}{\sigma_k}\frac{\partial k}{\partial x_k}\right] + \nu_t\left(\frac{\partial U_i}{\partial x_k} + \frac{\partial U_k}{\partial x_i}\right)\frac{\partial U_i}{\partial x_k} - \epsilon \tag{4.14}$$

$$\frac{D\epsilon}{Dt} = \frac{1}{\rho}\frac{\partial}{\partial x_k}\left[\frac{\nu_t}{\sigma_\epsilon}\frac{\partial \epsilon}{\partial x_k}\right] + C_1\nu_t\frac{\epsilon}{k}\left(\frac{\partial U_i}{\partial x_k} + \frac{\partial U_k}{\partial x_i}\right)\frac{\partial U_i}{\partial x_k} - C_2\frac{\epsilon^2}{k} \tag{4.15}$$

Thus the number of dependent variables increases to six (u, v, p, h, k, ϵ) and our mathematical system comprises of six partial differential equations.

4.10 Boundary Conditions for $k-\epsilon$ Model

Specifying appropriate boundary conditions for k and ϵ is not as straight forward as it is for velocities. Close to the wall there exists a small layer where the viscous effects dominate over the turbulence effects (viscous sublayer). The turbulent equations are not valid in this region. Modifications have been made to $k-\epsilon$ equations to make them valid over the whole region called low Reynolds number models [Launder, 1974]. But a more popular way is the use of wall functions in specifying the boundary conditions. Dirichlet boundary conditions for k and ϵ are not specified on the wall but at one grid point away from the wall (Fig.4.1). Close to the wall universal velocity distribution is assumed to be valid and the shear stress is calculated from the velocity at point P.

$$u_* = u_P \frac{\kappa}{ln\left(E\frac{u_* y_P}{\nu}\right)} \tag{4.16}$$

The quantity k_P, the value of k at the grid point P, is computed by assuming that the generation and dissipation of energy are equal in the wall layer where the shear stress is uniform and the length scale is proportional to the distance from the wall.

$$k_P = \frac{u_*^2}{\sqrt{C_\mu}}, \quad \epsilon_P = \frac{u_*^3}{\kappa y_P} \tag{4.17}$$

E is a function of wall roughness and is equal to 9.0 for smooth walls. Use of wall functions helps us jump the layer in which the gradients are very large and hence is

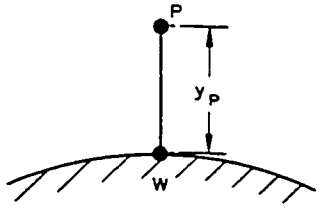

Figure 4.1: The near-wall nodes.

computationally advantageous. Moreover, information pertaining to factors such as wall roughness, pressure gradient, curvature etc. can be introduced through these wall functions.

At the free surface the normal gradients of k and ϵ are normally taken to be zero. Usually at the inlet the state of turbulence of the flow entering the test domain is not known. Thus imposing boundary conditions for k and ϵ is difficult. One way is to take the value of k as a percentage of the inlet kinetic energy, $k_{in} = fU_{in}^2$. Rahman(1991) took the value of f to be 0.0045. The value for ϵ can be estimated from the value of k assuming the mixing length to be $0.09H_{in}$, giving $\epsilon_{in} = C_\mu k_{in}^{3/2}/(0.09H_{in})$. At the exit plane the gradients of k and ϵ could be taken to be zero.

4.11 Free Surface Effects on Turbulence Structure in Open Channel Flow

When the turbulent eddies in a water flow impinge on the water surface, they cause a slight upward deflection of the surface which, in turn, generates an excess hydrostatic pressure pushing back the eddies. Hence, the vertical turbulent motion is damped by the presence of a free surface and, due to continuity, the fluctuations parallel to the surface are increased. Both the surface damping of the vertical fluctuations and the reduction of the turbulent length scale inhibit the vertical momentum transport by the turbulent motion so that the eddy viscosity is reduced near a free surface. In open channel flow, the eddy viscosity has typically a parabolic distribution while for closed channel flow the eddy viscosity does not decrease much towards the symmetry plane. To simulate the free surface effects on turbulence Celik(1984) suggested imposing the boundary condition for ϵ on the free surface as $\epsilon_s = \frac{k_s^{3/2}}{0.18H}$ instead of the symmetry condition, where H is the channel depth.

4.12 Surface Roughness

The channel bed is usually very irregular and rough. The effective height of the irregularities forming the roughness elements can be represented in terms of the equivalent sand roughness height, k_s. The ratio k_s/R of the roughness height to the hydraulic radius is known as the relative roughness. If the roughness elements are considerably small and are submerged within the laminar sublayer then the flow is considered to be hydraulically smooth and roughness has no effect on the velocity profile. In connection with flow in pipes or on flat plates at zero incidence, Schlichting gives the following condition for a surface to be hydraulically smooth:

$$\frac{u_* k_s}{\nu} < 5 \quad \text{or} \quad k_s < \frac{5\nu}{u_*} \tag{4.18}$$

where u_* is the friction velocity. If the roughness height is greater than the critical value, the roughness elements will have sufficient magnitude and angularity to extend their effects beyond the laminar sublayer through and thus to disturb the flow in the channel. The surface is therefore said to be rough. In rough channels, the velocity distribution will depend on the form and size of the roughness projections, and a stable laminar sublayer can no longer be formed. The universal velocity distribution can be written as:

$$\frac{u}{u_*} = \frac{1}{\kappa} ln \frac{9 y u_*}{\nu}, \text{ for smooth surfaces, } \frac{k_s u_*}{\nu} < 5 \tag{4.19}$$

$$\frac{u}{u_*} = \frac{1}{\kappa} ln \frac{30 y}{k_s}, \text{ for rough surfaces, } \frac{k_s u_*}{\nu} > 5 \tag{4.20}$$

Usually there is a range $5 < k_s u_*/\nu < 70$ in which both the laminar viscosity and surface roughness have an effect on the flow and is called the transition regime. But, this transition zone has been neglected by us as there is no available formula for universal velocity distribution in this regime.

Chapter 5

ARBITRARY LAGRANGIAN EULERIAN METHOD

With the turbulence modeling also complete, the system of equations are ready to be solved. In this chapter we discuss the method by which we overcome the problem posed by the changing free surface.

One of the reasons why open channel flow is so difficult to solve is that the free surface changes with time. Thus the computational domain is not known *apriori* and must be computed as part of the solution. Boundary conditions must be applied at a surface whose location is unknown. This introduces additional nonlinearity into the already nonlinear Navier Stokes equations.

5.1 Eulerian and Lagrangian view points

Traditionally fluid flow has been described using one of the following view points namely, Eulerian or Lagrangian. In the *Eulerian* view point attention is focused on some point in space and the changes in the fluid are described as functions of time at this point[Hirt(1974), Kawahara(1984), Ramaswamy(1990)]. In this method the fluid can undergo arbitrarily great distortions without loss of accuracy and outflow walls are particularly easy to handle. However, local resolution is difficult to achieve, and interfaces become blurred.

In the *Lagrangian* view point attention is focused on an infinitesimal fluid element and the changes in this fluid element are expressed as functions of time [Ramaswamy(1987), Hirt(1970)]. Lagrangian methods permit accurate treatment of

relatively low-amplitude free surface motions. In addition, they are easy to modify for multimaterial studies and the incorporation of surface-tension effects. Their principal disadvantage is that accuracy breaks down when distortions are large.

5.2 ALE View Point

A new technique called Arbitrary Lagrangian Eulerian (ALE) method has been developed which combines the advantages of purely Eulerian and purely Lagrangian view points without their disadvantages [Ramaswamy(1990), Hirt(1974)]. The nodal points of the mesh are moved independently of the fluid motion in this procedure. Because of the Lagrangian aspects of this technique, it is applicable to free surface flows, but it also retains the ability of Eulerian techniques to overcome undesirable grid distortions often associated with Lagrangian methods.

Changing the frame of reference changes the time derivatives. In the case of Eulerian approach acceleration of any quantity is given as:

$$\frac{\partial}{\partial t} + \mathbf{u} \cdot \nabla \quad : \quad \text{Eulerian time derivative} \tag{5.1}$$

Whereas in Lagrangian approach since the grid particle move along with fluid particle the convective terms disappear and the time derivative becomes:

$$\frac{\partial}{\partial t} \quad : \quad \text{Lagrangian time derivative} \tag{5.2}$$

In ALE method the grid points move independently of the fluid particles and hence the ALE time derivative becomes:

$$\frac{\partial}{\partial t} + (\mathbf{u} - \mathbf{w}) \cdot \nabla \quad : \quad \text{ALE time derivative} \tag{5.3}$$

where $\mathbf{w}$ is the velocity of the grid point. In Eulerian approach the grid points are fixed and hence $\mathbf{w} = 0$ whereas in Lagrangian approach the grid points move along with fluid particles, i.e., $\mathbf{w} = \mathbf{u}$ and the convective terms disappear. Thus the Lagrangian and Eulerian view points can be seen as special cases of ALE view point.

5.3 Free surface on vertical spines

We are interested in using ALE approach to solving open channel flow problems. Physical domain generally consists of an inlet or upstream end where the flow enters, an exit or downstream end through which the fluid flows out, a bed-water interface at the bottom and a water-air interface at the top. For these type of problems it is more easier to let the grid points move in the vertical direction but restrict them in the horizontal direction. That is we could visualize the free surface to be floating on vertical spines as shown in Fig5.1 This is not a new approach and has already been used by some investigators previously [Saito(1981), FIDAP(1991)]. Since the velocity gradients are large near the bed it is desirable to have closer mesh spacing near the wall. This is incorporated by distributing the grid points in a sigma stretched fashion. After each update of the free surface the grid points are redistributed on the spines in a similar manner. Due to this the nodes retain the same aspect ratio as set up by the initial mesh.

5.4 Governing Equations in ALE Formulation

As already stated the time derivatives in the ALE description are different from the Eulerian description. Thus the mathematical system to be solved using ALE description becomes:

$$\frac{\partial u}{\partial x} + \frac{\partial v}{\partial y} = 0 \tag{5.4}$$

$$\frac{\partial u}{\partial t} + u\frac{\partial u}{\partial x} + (v - w_y)\frac{\partial u}{\partial y} = gsin\theta - \frac{1}{\rho}\frac{\partial p}{\partial x} + \nabla \cdot (\nu + \nu_t)\nabla u \tag{5.5}$$

$$\frac{\partial v}{\partial t} + u\frac{\partial v}{\partial x} + (v - w_y)\frac{\partial v}{\partial y} = -gcos\theta - \frac{1}{\rho}\frac{\partial p}{\partial y} + \nabla \cdot (\nu + \nu_t)\nabla v \tag{5.6}$$

$$\frac{\partial h}{\partial t} + u\frac{\partial h}{\partial x} = v \tag{5.7}$$

$$\frac{\partial k}{\partial t} + u\frac{\partial k}{\partial x} + (v - w_y)\frac{\partial k}{\partial y} = P_k - \epsilon + \nabla \cdot \frac{\nu_t}{\sigma_k}\nabla k \tag{5.8}$$

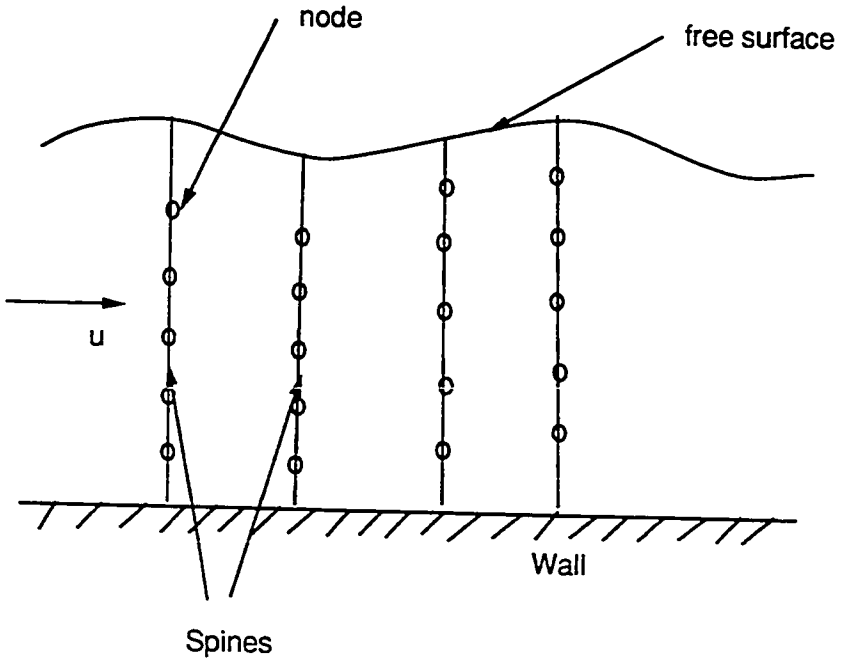

Figure 5.1: Free surface resting on vertical spines

$$\frac{\partial \epsilon}{\partial t} + u\frac{\partial \epsilon}{\partial x} + (v - w_y)\frac{\partial \epsilon}{\partial y} = \frac{\epsilon}{k}P_k - C_1\frac{\epsilon}{k}\epsilon + C_2\nabla \cdot \frac{\nu_t}{\sigma_\epsilon}\nabla\epsilon \tag{5.9}$$

where $P_k = \nu_t \frac{\partial u_i}{\partial x_k}\left(\frac{\partial u_i}{\partial x_k} + \frac{\partial u_k}{\partial x_i}\right)$. The boundary conditions remain the same. It is to be noted that since the nodes don't move in the x-direction, $w_x = 0$ and is not shown in the above equations.

Chapter 6

NUMERICAL METHOD

The next step in our flow modeling process is to solve the nonlinear partial differential equations governing the flow. Analytical solutions are almost impossible due to nonlinearities. The only other way they could be solved is through numerical means. The philosophy behind most numerical methods is to convert the partial differential equations into a set of algebraic equations which can be solved on the digital computers. The most common ways of doing this is finite difference method, finite element method and finite volume method. Finite element method has some very desirable properties the most important among them being the capability to handle irregular geometries. Thus we chose to use finite element method to solve our equations.

6.1 Selecting The Dependent Variables

The variables u, v and p are called the primitive variables. However, we can define other mathematical entities such as stream function, vorticity and velocity potential in terms of these primitive variables. Prominent among the various formulations for Navier-Stokes equations are:

- Stream function-vorticity formulation [Cheng(1972), Baker(1973)].
- Velocity-Pressure formulation [Harlow(1965), Chorin(1967)].
- Penalty function formulation [Iga, 1989].

All the above formulations have their own advantages and disadvantages and are to be chosen depending on the nature of the problem. Stream function-vorticity formulation

has the advantage of satisfying continuity equation exactly and of not having to solve for pressure. But it is not possible to define a stream function in three-dimensions and hence has not been used by us. The disadvantage with penalty formulation is choosing the penalty parameter whose selection could prove to be very tricky. Hence the primitive variable formulation in which the dependent variables are velocity and pressure has been used in our flow model. The boundary conditions, especially at the free surface are easier to handle using the primitive variables formulation.

6.2 Solving For Pressure

Apart from the fact that Navier-Stokes equations are non-linear, the absence of pressure in the continuity equation in the case of incompressible flow poses the biggest problem. In compressible flow the time derivative of pressure appears in the continuity equation and evaluation of pressure does not pose as much challenge as it does in incompressible flows. Direct solution of u, v and p would require that approximating spaces satisfy the Babuska-Brezzi stability criteria. In order to satisfy the Babuska-Brezzi stability criteria the approximating spaces for the pressure are chosen to be of lower order than those used for velocities, i.e., staggered grids(Fig.6.1e) or mixed formulations need to be used.

However, if u, v and p are solved for in a decoupled manner, then we could obtain stable solution using both staggered(Fig.6.1e) and non-staggered grids(Fig.6.1f) [Zienkiewicz, 1991]. There are two common formulations for the numerical solution of the incompressible Navier-Stokes equations in primitive variables, the artificial compressibility and the pressure Poisson equation methods. The velocity field is calculated from the time dependent momentum equation using time marching techniques, while each method employs a different equation to compute the pressure. In the artificial compressibility method, a time derivative of the pressure is added to

the continuity equation and the incompressible field is treated as compressible during transient calculations [Chorin, 1967]. On the other hand, the pressure Poisson method replaces the continuity equation with a second-order elliptic Poisson equation for the pressure [Harlow, 1965]. However, if artificial compressibility method is chosen then equal order approximations for pressure and velocity would require that a fourth order pressure derivative be added to the continuity equation to stabilize the solution. But no such stabilizing term need to be added if pressure is obtained using Poisson equation as the stabilizing term is inherent in the procedure. We chose to use the pressure Poisson equation since it was felt that artificial compressibility method may impose a more stringent restriction on the time step.

6.3 Fractional Step Method

Velocities and pressure are decoupled and solved in a sequential manner using Fractional Step Method (Projection Method) first proposed by Chorin(1968). Starting with the initial solution $u(x, y, 0) = u_0$, the Navier-Stokes equations are solved successively as follows:

Step 1:

The intermediate velocities, $\tilde{u_i}^{n+1}$ are evaluated neglecting the pressure gradient terms in the momentum equation.

$$\frac{\tilde{u}_i^{n+1} - u_i^n}{\Delta t} - \frac{\partial}{\partial x_j}(\nu + \nu_t)\frac{\partial \tilde{u}_i^{n+1}}{\partial x_j} = -(u_j^n - w_j^n)\frac{\partial u_i^n}{\partial x_j} + f_i^n \tag{6.1}$$

The advection terms are treated explicitly using the Euler forward scheme. The viscous terms are treated implicitly. Hence this procedure can be said to be semi-implicit in time. In this step the dirichlet and Neumann boundary condition for u_i are imposed. The intermediate velocities ($\tilde{u_i}^{n+1}$) however are not divergence free and need to be corrected.

Step 2:

Pressure is evaluated using the Poisson equation which is obtained by taking divergence both sides of the Navier-Stokes equations and imposing the divergence free condition on the new time step velocities, u_i^{n+1}.

$$p_{,ii}^{n+1} = \frac{1}{\Delta t}\frac{\partial \tilde{u}_j^{n+1}}{\partial x_j} \tag{6.2}$$

Step 3:

The pressure gradient terms previously omitted in the evaluation of $\tilde{u}_i^{n+1}$ are added back.

$$\frac{u_i^{n+1} - \tilde{u}_i^{n+1}}{\Delta t} = -\frac{1}{\rho}\frac{\partial p^{n+1}}{\partial x_i} \tag{6.3}$$

Evalualtion of u_i^{n+1} and p^{n+1} mark the end of the time step calculation and the procedure is repeated every time step.

6.4 Spatial Discretization

The previous section dealt with the temporal discretization strategy for the Navier-Stokes equations. Spatial discretization in finite element method involves the dividing of the physical domain into small elements which could be of any shape like triangles, rectangles etc. as shown in Fig.6.1. The unknown function is assumed to have a polynomial variation within the element and is expressed in terms of the nodal variables. Depending on the type of polynomial variation desired we need to place that many nodes in each element. For example as shown in Fig.6.1 we could have either 3-noded or 6-noded triangles, in the former case the variables are assumed to be linear within the element, whereas in the latter case they are assumed to be quadratic. For our discretization we chose 3-noded triangle elements. Finite elements offer a rich variety of elements that can be used for spatial discretization as explained very well in Huebner(1982). With this spatial discretization and use of Galerkin weighted residual formulation we arrive at a system of matrix equations.

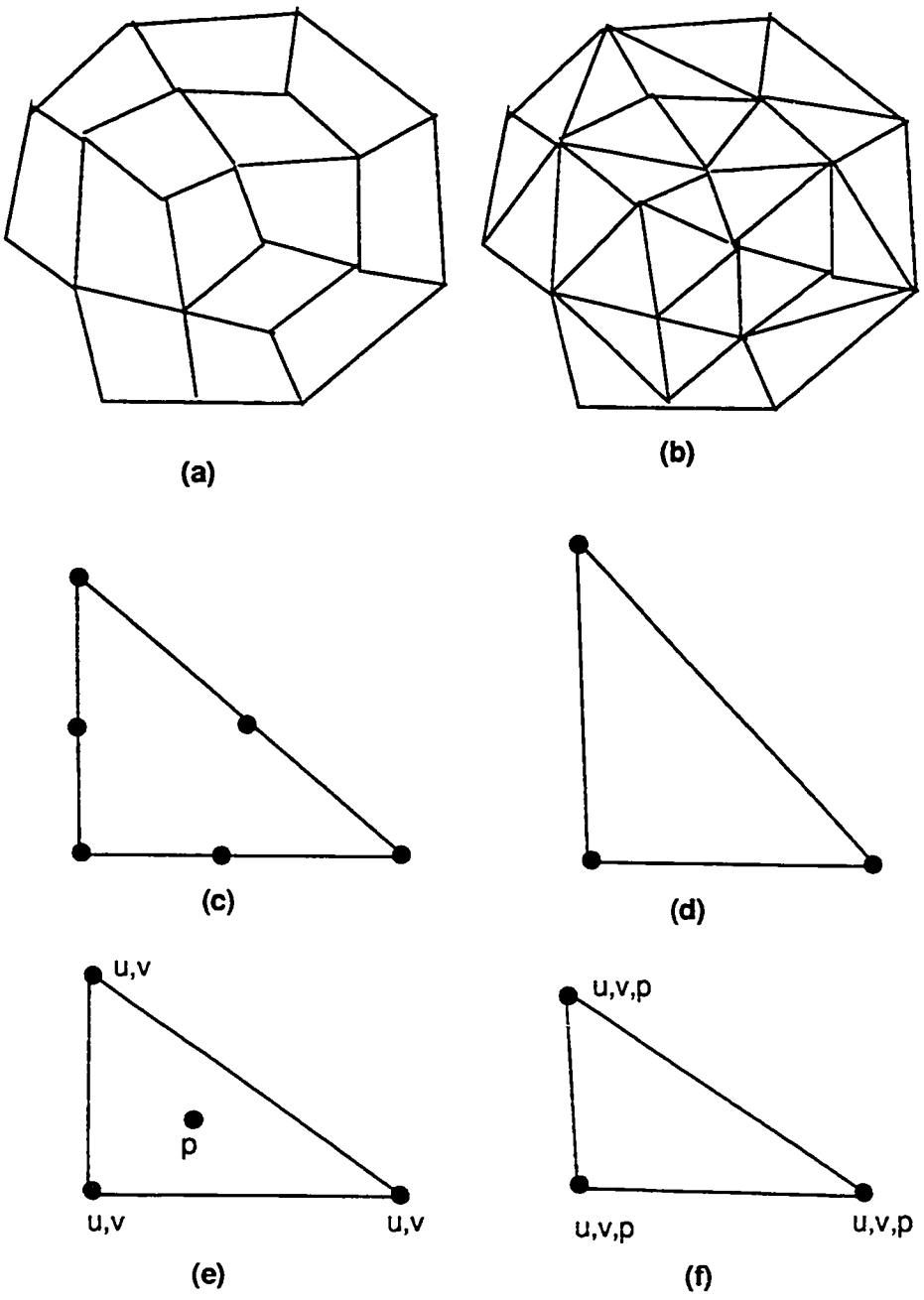

Figure 6.1: Finite element discretization: (a) rectangles,(b) triangles, (c) 6-noded triangles, (d) 3-noded triangle, (e) staggered grid, (f) non-staggered grid

6.5 Satisfying Continuity Equation Exactly

It has been shown that the continuity equation is satisfied to machine accuracy in the case of staggered grids. But this is not case if equal order approximation for pressure and velocity is used (non-staggered grid). The error is equal to a source term proportional to the fourth order spatial derivative of pressure. This mass balance error has been shown to be equal to [Sotiropoulos, 1991]:

$$D_{i,j} = -\frac{\Delta t}{4}[\Delta x^2 \delta_{xxxx} P + \Delta y^2 \delta_{yyyy} P + \Delta x^2 \delta_{xx}(u \delta_{xx} u) + \Delta y^2 \delta_{yy}(v \delta_{yy} v) + \text{cross derivative terms}] \quad (6.4)$$

Above result has been derived for finite difference central difference discretizations in space. It is not unreasonable to expect it to be true for Galerkin finite element method also.

Equal order approximation or non-staggered grids have been used by us. Due to this reason careful attention has been paid to mass conservation. For most of our simulations we didn't have an error grater than 3% in mass balance. This could partly be due to the proper selection of time step and mesh spacing. But our formulation also has some features of staggered grid in it. The pressure was split into a hydrostatic part and a non-hydrostatic part.

$$p = \rho g(h(x) - y) + \tilde{p} \quad (6.5)$$

where $h(x)$ is the free surface height from a datum and $\tilde{p}$ is the correction to the hydrostatic pressure. This is done due to the fact that in open channel flow pressure is nearly hydrostatic with significant deviations from this only in areas of rapid acceleration and recirculation. It is only for $\tilde{p}$ that we solve the pressure Poisson equation whereas the hydrostatic part being already known from the free surface height is used in the momentum equations straight away. This procedure of splitting the pressure and it being close to hydrostatic pressure could have also helped in keeping the mass

balance errors to a minimum. However, this aspect needs further research before definite conclusions can been drawn.

6.6 Solvability Conditions for the Navier-Stokes Equations

Let the initial condition be given by

$$u(x, y, 0) = u_0(x, y) \tag{6.6}$$

Then it is required that

$$n \cdot u_0 = n \cdot \hat{u} \tag{6.7}$$

and

$$\nabla \cdot u_0 = 0 \tag{6.8}$$

in order that a solution exist. $\hat{u}$ is the dirichlet boundary condition for the velocity. Navier-Stokes equations are ill-posed if any of the above two conditions are violated [Gresho, 1987].

6.7 Error Estimates for Fractional Step Method

Deriving error estimates for the fractional step scheme is not straight forward. One of the reasons is when the intermediate velocity $\tilde{u}_i^{n+1}$, is projected onto the divergence free space H, u_i^{n+1} only lies in H but does not necessarily satisfy the boundary conditions for velocity[Shen, 1992]. Shen(1992) has been able to show that both $\tilde{u}_i^{n+1}$ and u^{n+1} are weakly first order approximations to $u(t_{n+1})$ and that p^{n+1} is weakly oder $\frac{1}{2}$ to $p(t_{n+1})$.

6.8 Artificial Diffusion

In convection dominated problems Galerkin formulation requires that the mesh be fine in order to avoid oscillations in the solution. There are various ways this can be overcome, for eg., using streamline upwind Petrov Galerkin (SUPG) method devel-

oped by Brooks(1982). We applied artificial diffusion using selective mass lumping. The approach has features similar to Lax-Friedrichs scheme in the finite difference context. The Lax-Friedrichs scheme for the one-dimensional linearized convection equation $u_t + au_x = 0$ is given by:

$$u_i^{n+1} = \frac{1}{2}(u_{i+1}^n + u_{i-1}^n) - \frac{\sigma}{2}(u_{i+1}^n - u_{i-1}^n) \tag{6.9}$$

where $\sigma = \frac{a\Delta t}{\Delta x}$ is the CFL number. From the truncation error analysis [Hirsch,1988] it can be shown that the scheme has artificial diffusion α given by:

$$\alpha = \frac{a}{2\sigma}\Delta x(1-\sigma^2) = \frac{\Delta x^2}{2\Delta t}(1-\sigma^2) \tag{6.10}$$

Comparing with the Galerkin finite element formulation, eqn.6.9 can be viewed as lumped mass matrix on the LHS and consistent mass matrix on the RHS.

This same idea is used by us, namely selective mass lumping. Let M_L and M_R be the mass matrices on the LHS and RHS respectively.

$$M_L = \alpha_L M_D + (1-\alpha_L)M_C \tag{6.11}$$

$$M_R = \alpha_R M_D + (1-\alpha_R)M_C \tag{6.12}$$

where M_D and M_C are the lumped and consistent mass matrices respectively. α_L and α_R are the lumping parameters and take values 0 to 1. Choosing different values of α_L and α_R we obtain different levels of mass lumping. Through numerical experiments we choose α_L and α_R, just enough to achieve stable solution without excessive mass lumping which causes phase error and large numerical diffusion. Typical values of α_L and α_R used are:

- $\alpha_L = 0.1$ and $\alpha_R = 0.0$ in the calculation of intermediate velocities.
- $\alpha_L = 1.0$, and $\alpha_R = 0.9$ in the calculation of divergence free final time step velocities.
- $\alpha_L = 0.2$ and $\alpha_R = 0.0$ in the calculation of k and ϵ.
- $\alpha_L = 0.1$ and $\alpha_R = 0.0$ in the calculation of free surface.

6.9 Miscellaneous features

The procedure for flow simulation is shown in the form of a flow chart in Fig.6.2. The system of equations are solved by Cholesky factorization. All the computations are performed on the NCSC CRAY-YMP machine. The time step is selected automatically by the code based on the previous time step velocities. The criterion for stability are:

$$\Delta t \leq max\left[\frac{\Delta x}{|u|}, \frac{\Delta y}{|v|}\right]; \quad \text{CFL constraint} \tag{6.13}$$

$$\Delta t \leq \frac{\Delta x}{|u| + \sqrt{gh}}; \quad \text{surface gravity waves constraint} \tag{6.14}$$

It has been observed that the time step limit is imposed by the surface gravity waves. The mass matrix is lumped in the calculation of final velocities in projection scheme. This is done for computational convenience.

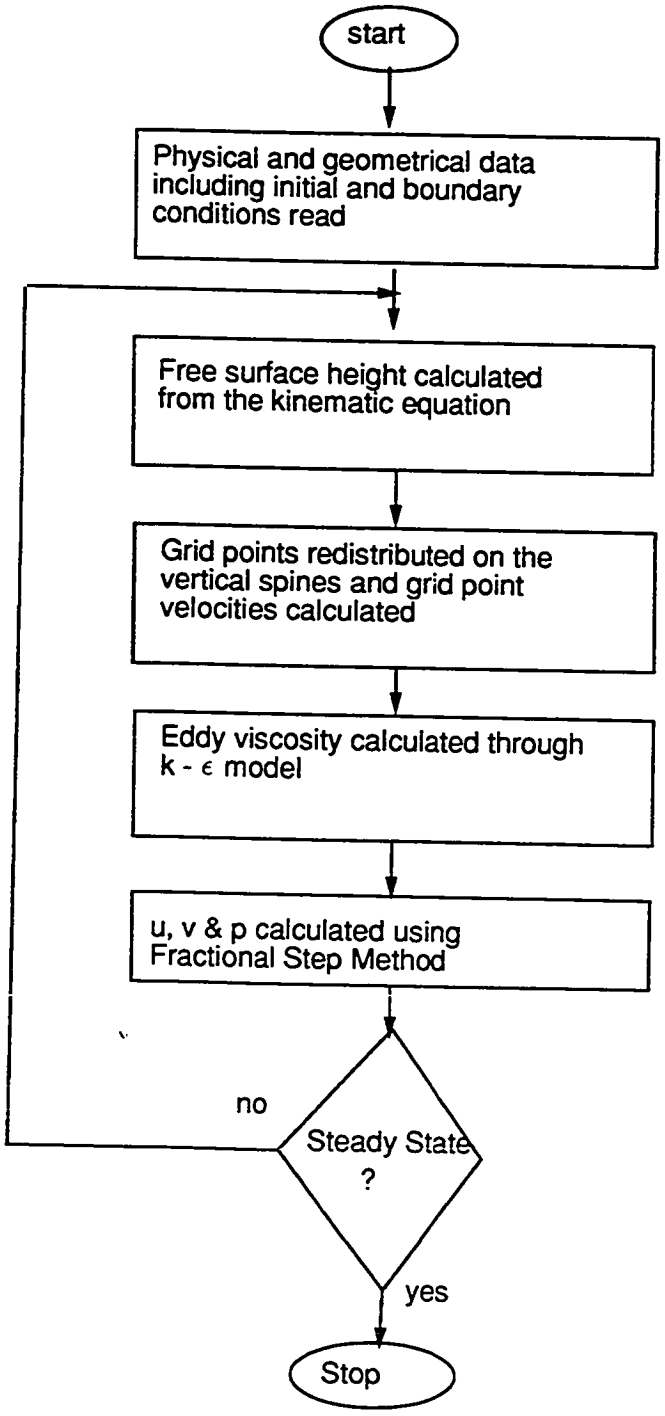

Figure 6.2: Procedure for Flow Simulation

Chapter 7

RESULTS AND DISCUSSION : OPEN CHANNEL FLOW SIMULATION

Unfortunately in open channel flow there are no good bench mark problems which can be used to validate codes and models. This is partly due to the wide variety of conditions in which they occur in nature. Operating conditions such as wall roughness, channel geometry etc. are site-specific and hence ready comparison with experimental data is difficult. Further most of the research in open channel flow simulation has been done using depth averaged models and hence not much information is available on the vertical structure of the flow.

In the absence of readily available experimental data and previous numerical results we had to set up our own model problems. To gain confidence in our results simple checks have been performed to verify that no physical principles such as conservation of mass or momentum is violated.

7.1 Flow over an Inclined Plane

The experimental problem chosen is flow over an inclined plane. A steady discharge of water is sent in at the upstream end of an inclined plane. At the downstream end, depending on whether the flow is restricted or not two different classes of problems develop. If no restriction is imposed the flow does not change character and remains supercritical through out. If a restriction on the flow height is imposed the flow changes from supercritical to subcritical and hydraulic jump is formed. Both types of problems have been investigated by us.

The various parameters governing the flow are: inlet height (H), length of the plane (L), discharge (Q), slope of the plane (θ) and wall roughness (k_s). Selecting Q and H automatically fixes the inlet Reynolds number(Re_{in}) and inlet Froude number (Fr_{in}).

$$Re_{in} = \frac{Q}{\nu} \; ; \; Fr_{in} = \frac{Q}{\sqrt{gcos\theta}H^{3/2}} \tag{7.1}$$

In order to reduce the number of variable parameters we chose to fix the inlet flow height to be $0.2m$ and length of the plane to be $20.0m$. Thus the nature of the flow is investigated by varying θ, k_s and Q.

At the inlet horizontal velocity computed from the logarithmic law is imposed. At the downstream end fully developed velocity profile condition is imposed. Due to the Galerkin formulation this boundary condition is taken care of in a natural way. The inlet turbulent kinetic energy is specified as a percentage of the inlet kinetic energy. The dissipation rate(ϵ) at the inlet is determined assuming a mixing length equal to $0.09H_{in}$. At the exit fully developed conditions are imposed for k and ϵ.

7.2 Numerical Experiments

We identified three numerical aspects of the code which need to be investigated.

- artificial diffusion through selective mass lumping
- mass and momentum balance
- mesh independency

For our numerical experimentation the operating conditions have been taken as, $Q = 0.50m^2/s$, $k_s = 0$, implying smooth wall and the inclination (θ) to be 0.01. These operating conditions give us $Re_{in} = 5.0 \times 10^5$ and $Fr_{in} = 1.78$.

In Fig.7.1 the effect of mass lumping is shown. The free surface profile shown is that obtained at the end of 50 time steps using a 61×21 mesh.. As can be seen the

numerical scheme without any selective mass lumping is unstable and in fact diverged after a few more time step calculations. Where as, even 10% differential mass lumping was enough to stabilize the scheme. 10% selective mass lumping means that the mass matrix on the LHS is lumped 10% more than the mass matrix on the RHS or that $\alpha_L - \alpha_R = 0.1$. Most of the results presented from here on or those obtained using 10% selective mass lumping.

At steady state the discharge at every cross-section (Q_x) must be the same and equal the inlet discharge (Q) or in other words $\frac{dQ(x)}{dx} = 0$. This is a good check to verify if mass is being conserved.

Integrating the steady state x-momentum equation across the cross-section, we obtain

$$Mom_x = \frac{dE_x}{dx} - gh(x)sin\theta + \tau_w = 0.0 \tag{7.2}$$

where

$$E_x = \int_0^{h(x)} u^2\, dy + \frac{1}{2} g cos\theta h^2(x) \tag{7.3}$$

E_x can also be seen as the sum of kinetic and potential energies at cross-section x. Mom_x represents the fact that the change in momentum is caused by the external forces, in this case, gravity and wall shear stress and when properly accounted for should equal zero. This is a good check to determine if momentum conservation is obeyed. In Fig.7.2 the mass and momentum conservation errors as percentages of inlet discharge and energy are plotted. The errors in conservation of mass and momentum are less than 1% with the maximum errors occuring at the inlet and exit.

The free surface profiles for different mesh spacings in the x-direction are shown in Fig.7.3. For the mesh size 41×21 the solution did not converge and was unstable, whereas for meshes 61×21 and 101×21 converged steady state solution could be obtained. As can be seen there is very little difference in the solution between 61×21

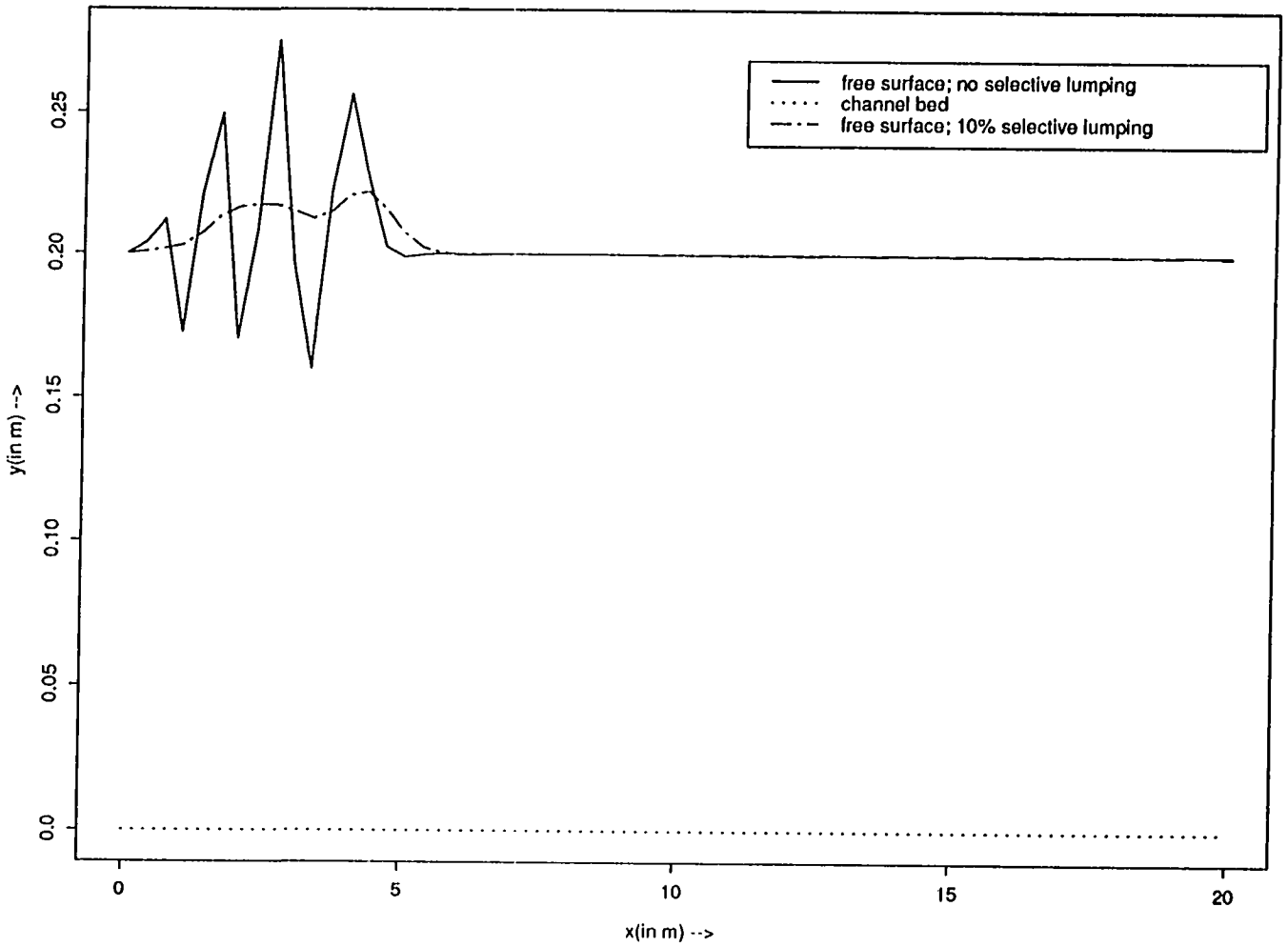

Figure 7.1: Effect of selective mass lumping

and 101×21 mesh. Thus 61 grid points in x direction is sufficient in the x-direction to get a stable converged solution.

Fig.7.4 shows the free surface profile for different grid points in y-direction. Unlike in x direction, in the vertical direction the grid points are distributed in a logarithmic manner as the velocity gradients are larger near the wall [Anderson, 1984]. The difference in solution between 61×21 and 61×31 is very little. For 61×11 the solution did not converge but exhibited oscillations.

Based on these numerical experiments we chose the grid size to be 61×21 and used 10% selective mass lumping in all mass matrices. These conditions have been used by us for all the subsequent runs. However in the simulation of hydraulic jump some of these conditions are changed and these aspects are discussed in the subsequent section on hydraulic jump. The fact that the mass and momentum are conserved fairly well is a sort of reassurance that at least no physical principle is being violated in our model. It has been observed that some of these aspects could become really important in areas where steep gradients exist. In the hydraulic jump simulation whose results will be presented in a later section large gradients do occur and these factors such as mass and momentum conservation become very important.

7.3 Supercritical Flow Simulation

Now that sufficient confidence has been obtained on the numerical procedure we can get into investigating the physics of the problem. As already mentioned the three parameters which are being controlled are Q, k_s and θ. Figs.7.5,7.6 and 7.7 show the effect of these three variables on the free surface profile. On the surface they seem to make sense qualitatively;

- increasing the slope would decrease the flow height since flow would be faster,

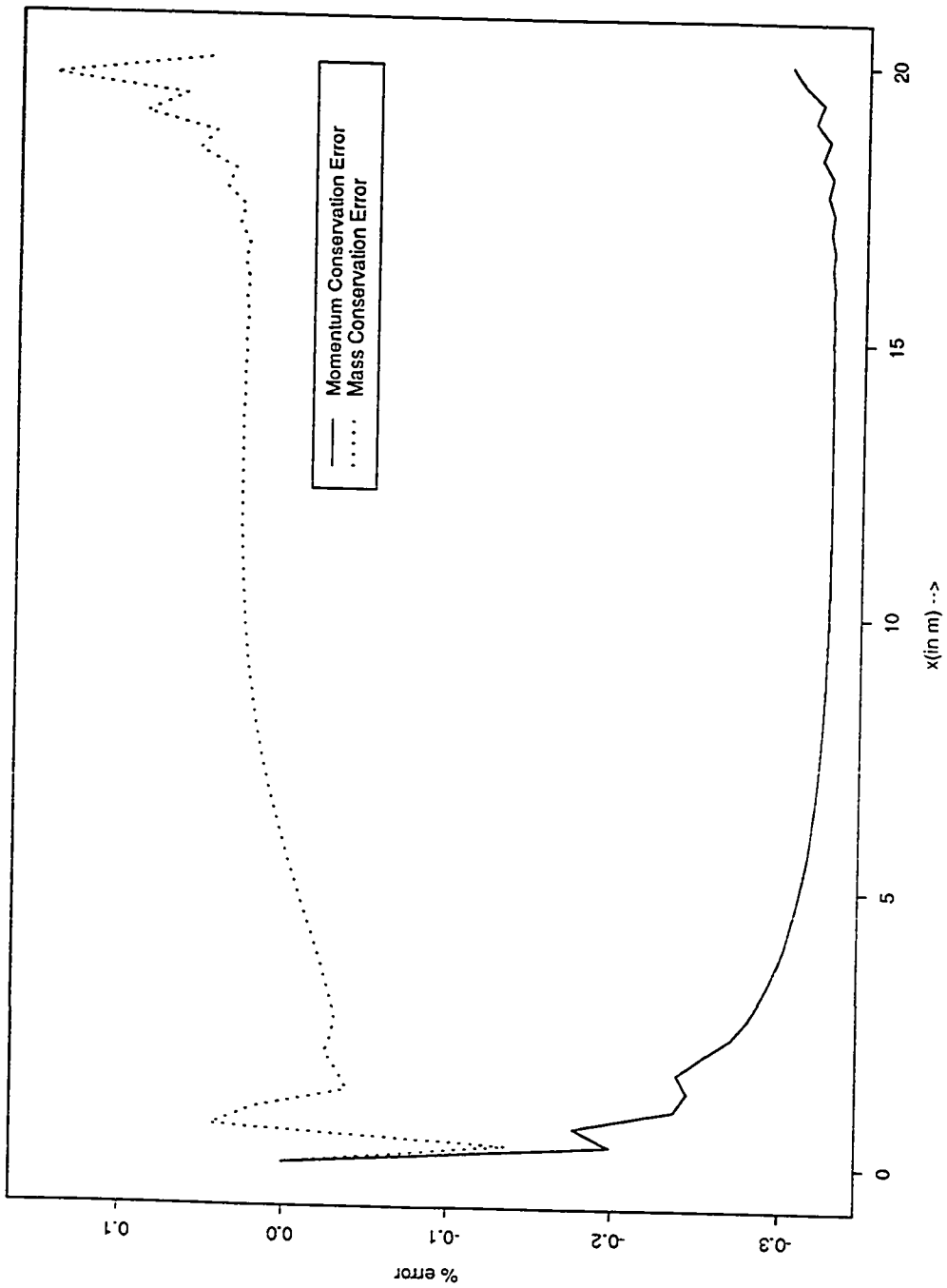

Figure 7.2: Percentage Errors of Mass and Momentum Conservation Laws

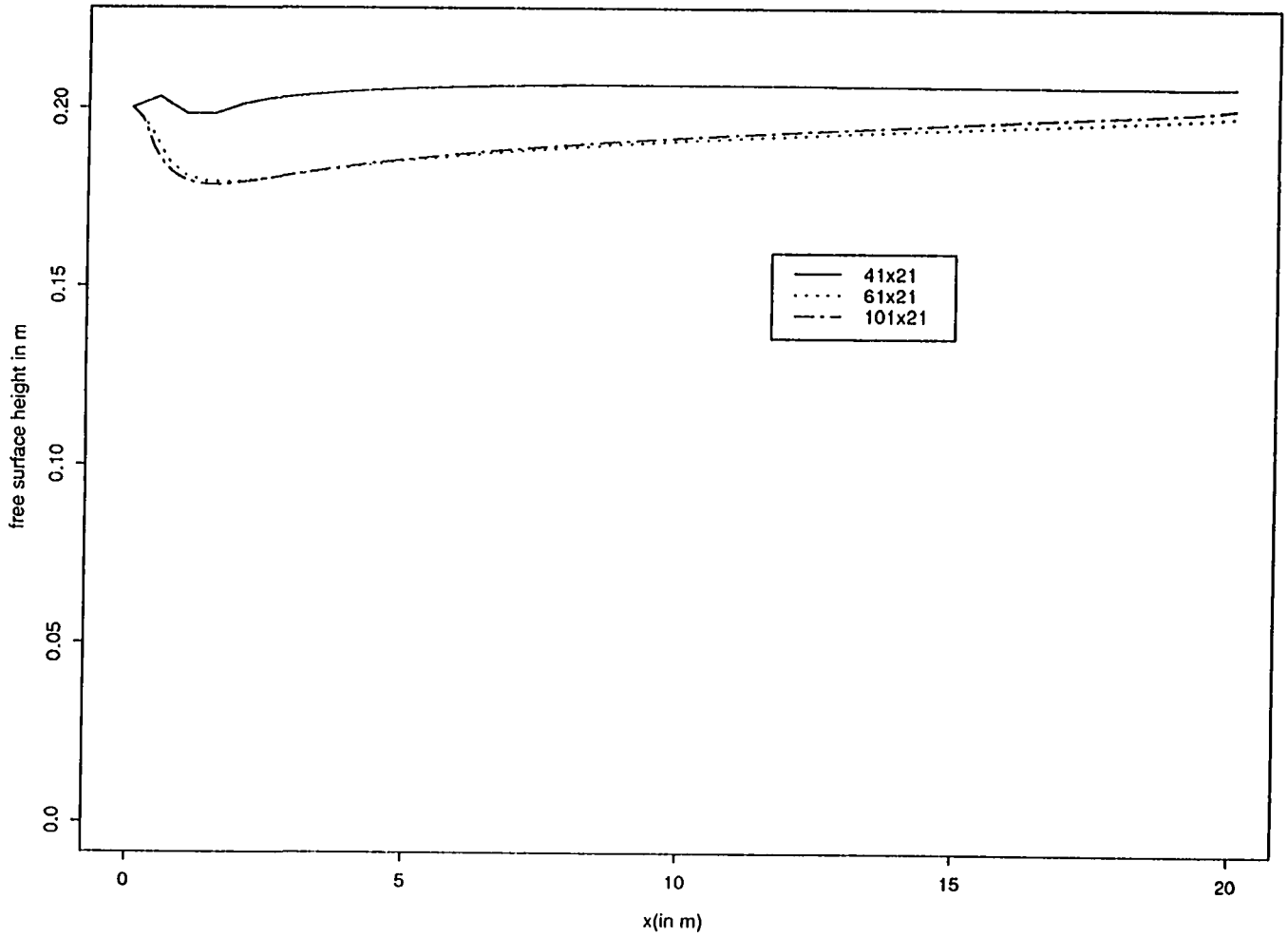

Figure 7.3: Free surface profiles for different mesh spacings in x-direction

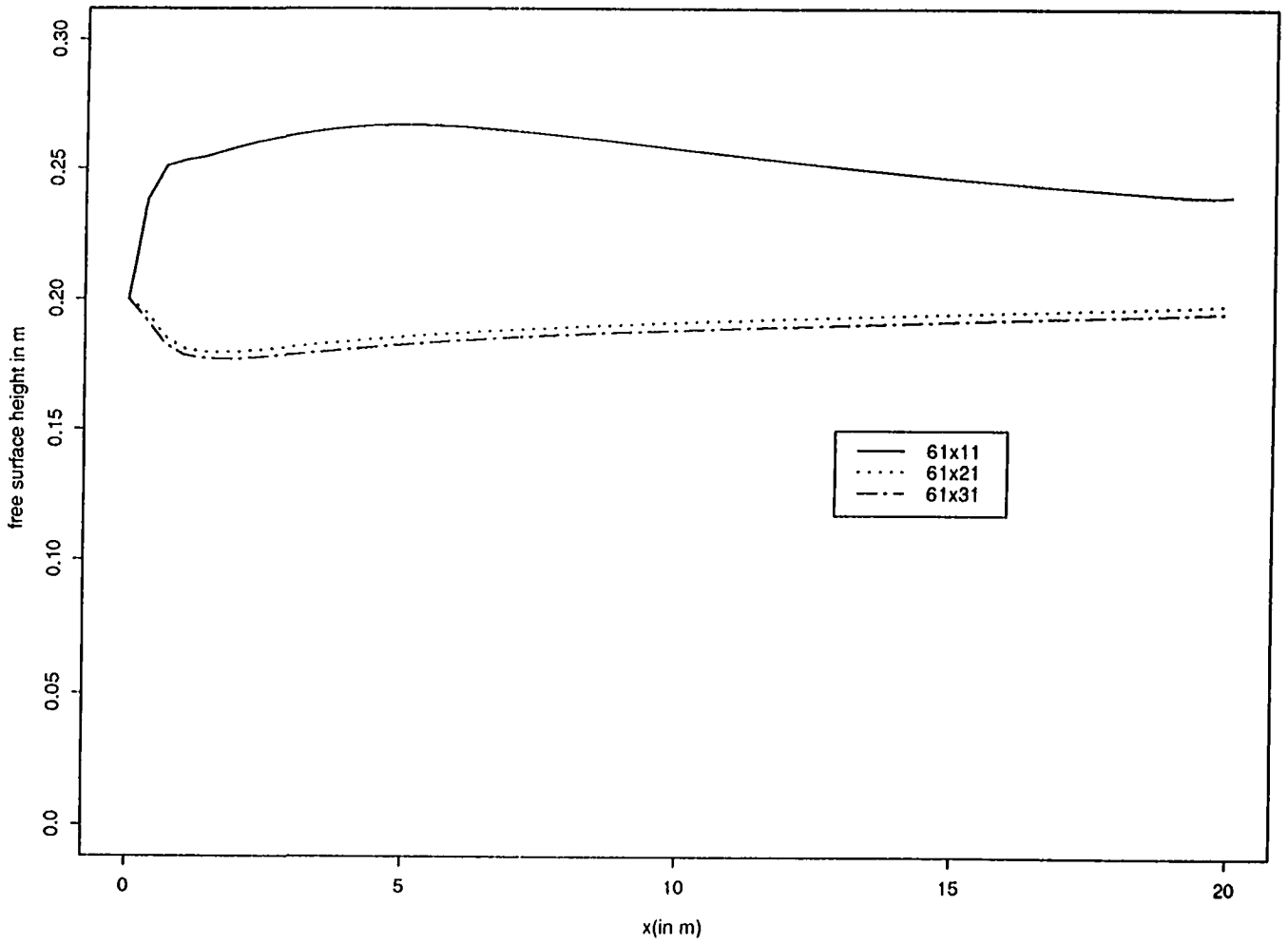

Figure 7.4: Free surface profiles for different mesh spacings in y-direction

- increasing the roughness would slow down the flow and consequently flow height would be more, and

- greater the discharge greater the flow height other conditions remaining same.

However they will need to be compared with experimental values if their quantitative correctness is to be verified. The velocity profile at $x = 10.0m$ is plotted in Fig.7.8 and compared with the logarithmic distribution and the Coles law. Coles law is the logarithmic law modified to take into effect the influence of pressure gradient on the velocity distribution. The agreement with both the laws is not good with Coles law performing only marginally better. The vertical profiles of k, ϵ and ν_t are shown in Fig.7.9. It can be seen that the eddy viscosity is parabolic in the bottom layer and becomes constant in the upper layers of the flow. However it has been observed that due to the turbulent fluctuations at the free surface the eddy viscosity decreases towards the free surface. This is enforced by imposing $\epsilon_s = \frac{k_s^{3/2}}{\kappa h}$ instead of symmetry boundary condition for ϵ. However, we have not applied this modified boundary condition for ϵ at the free surface in our simulations.

There are theoretical results and numerical experiments which state that supercritical flow with Froude number greater than a critical value(F_{cr}) is unstable. This value has been determined to lie some where between 1.5 and 2.0 depending on the conditions such as wall roughness, aspect ratio etc. [Sarma, 1991]. In our simulations of supercritical flow solution has been obtained for Froude numbers as high as 4.0. This could partly be due to the numerical damping we are enforcing to obtain stable solution. Thus our results for the free surface could be seen as the time mean value, whereas the instantaneous free surface height could be a fluctuating quantity. Another reason for our obtaining a stable solution could be that our mesh is not fine enough to capture the ripples. Our mesh spacing in the x-direction is $0.33m$ whereas

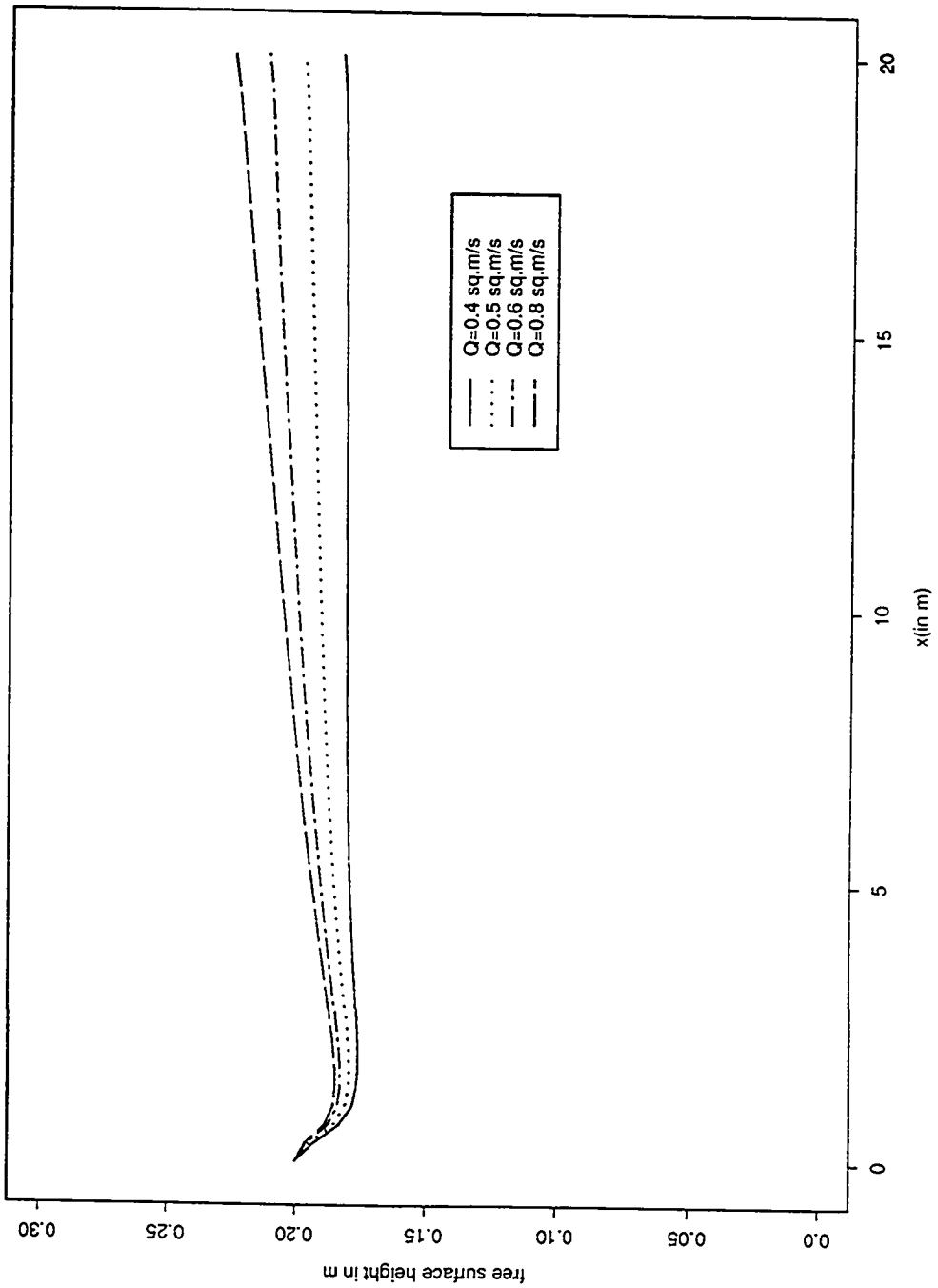

Figure 7.5: Effect of discharge on the free surface profile

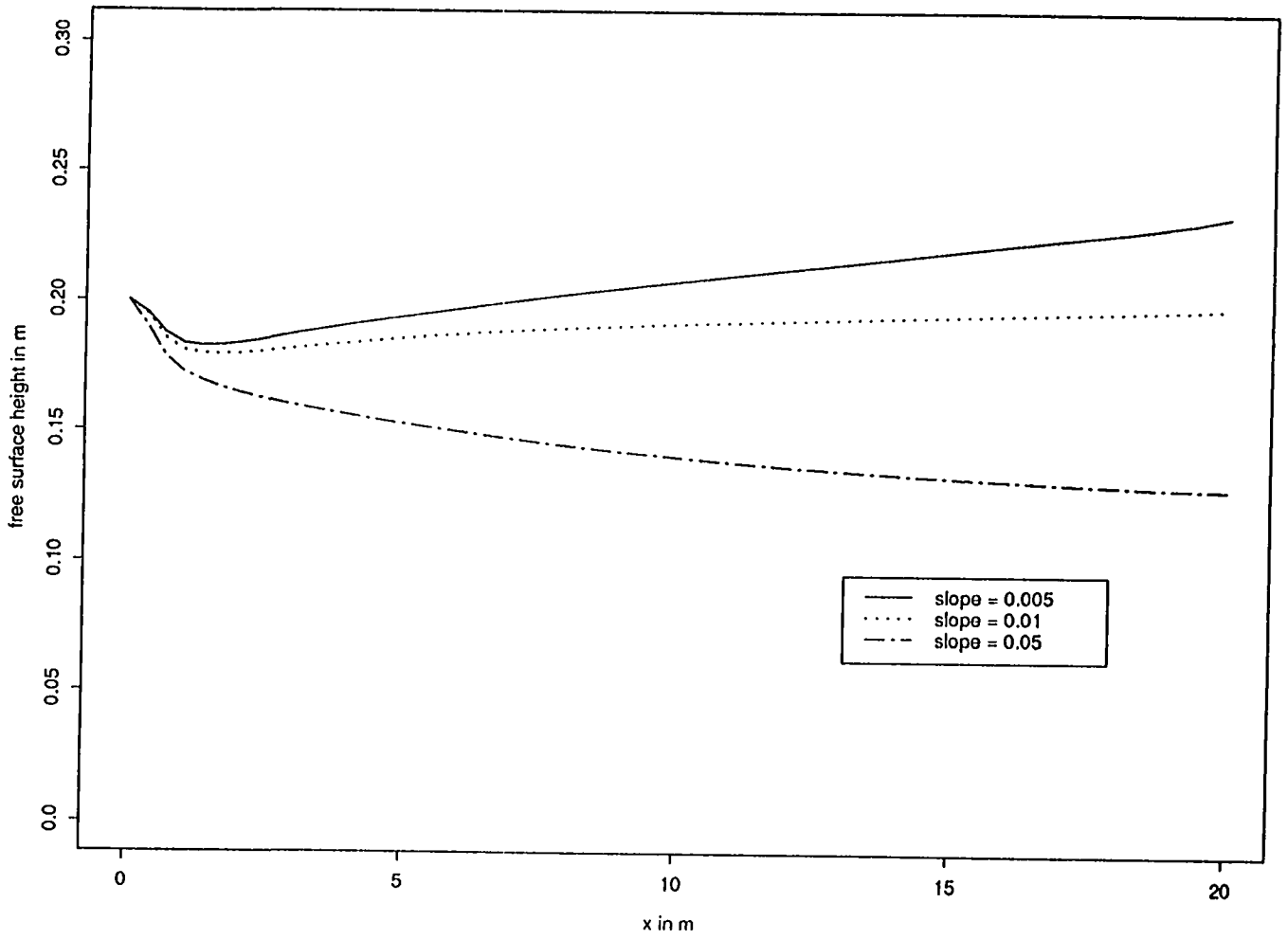

Figure 7.6: Effect of inclination on the free surface profile

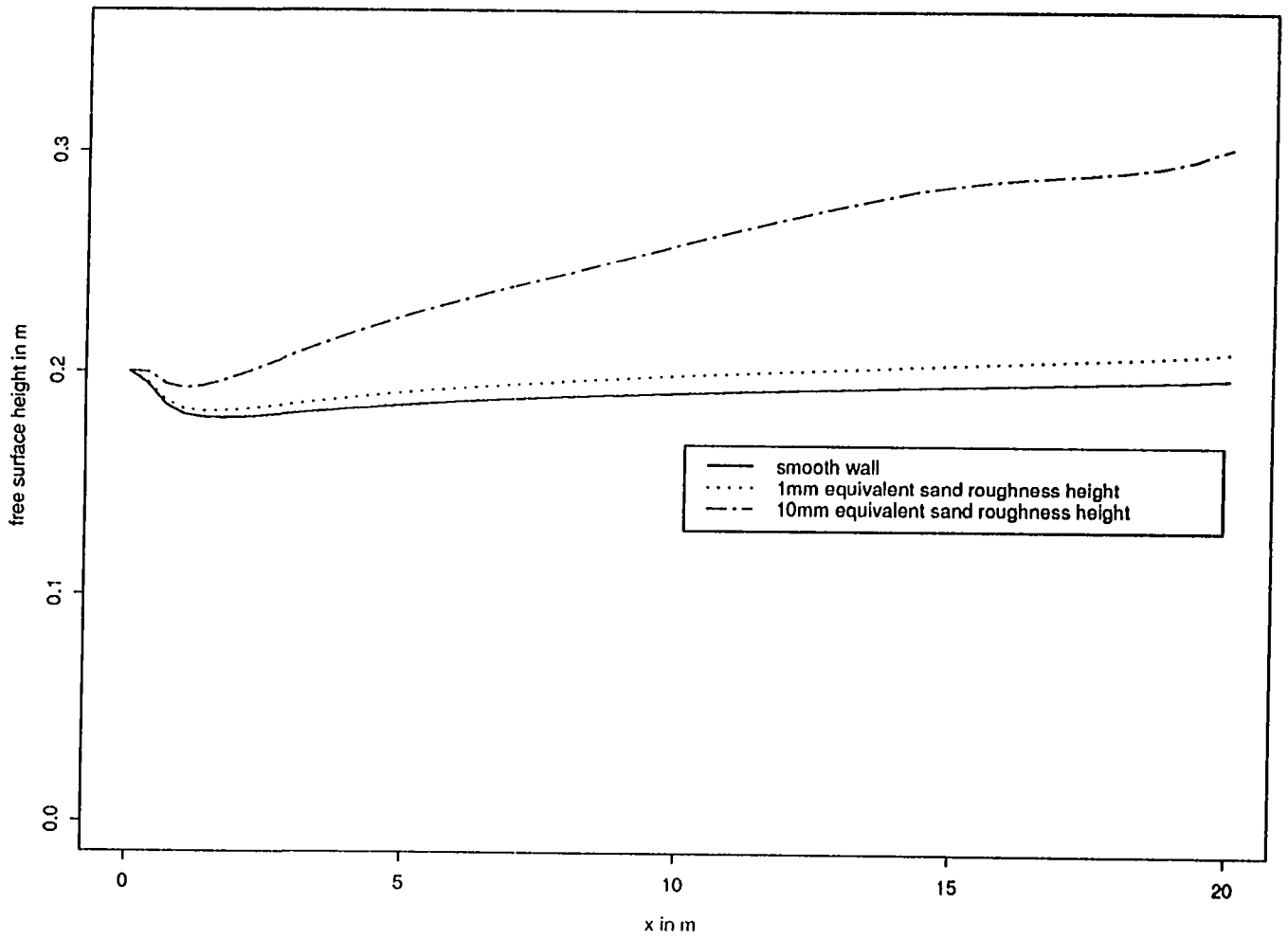

Figure 7.7: Effect of surface roughness on the free surface profile

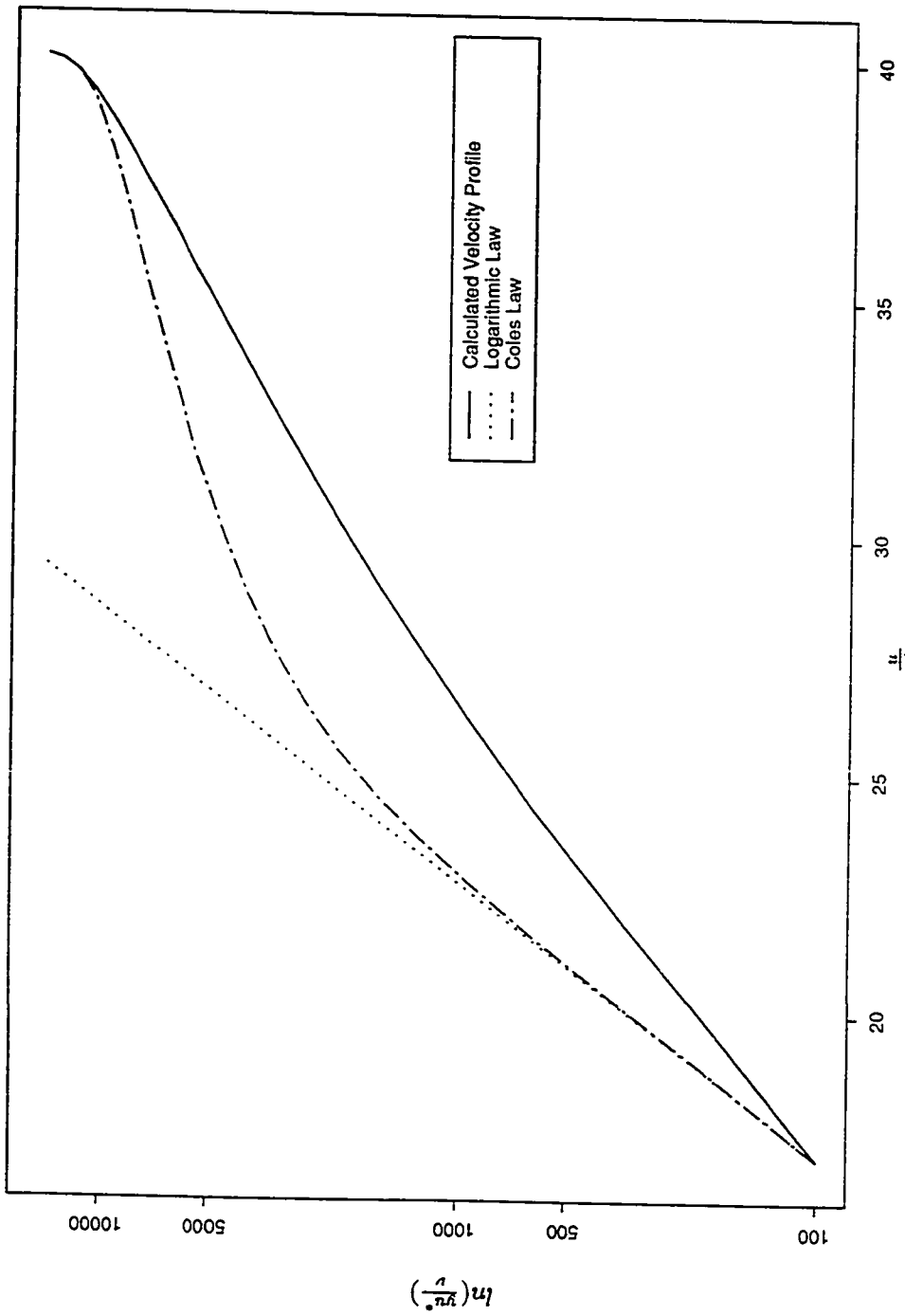

Figure 7.8: Velocity profile compared with logarithmic law and the Coles law at $x = 10.0m$.

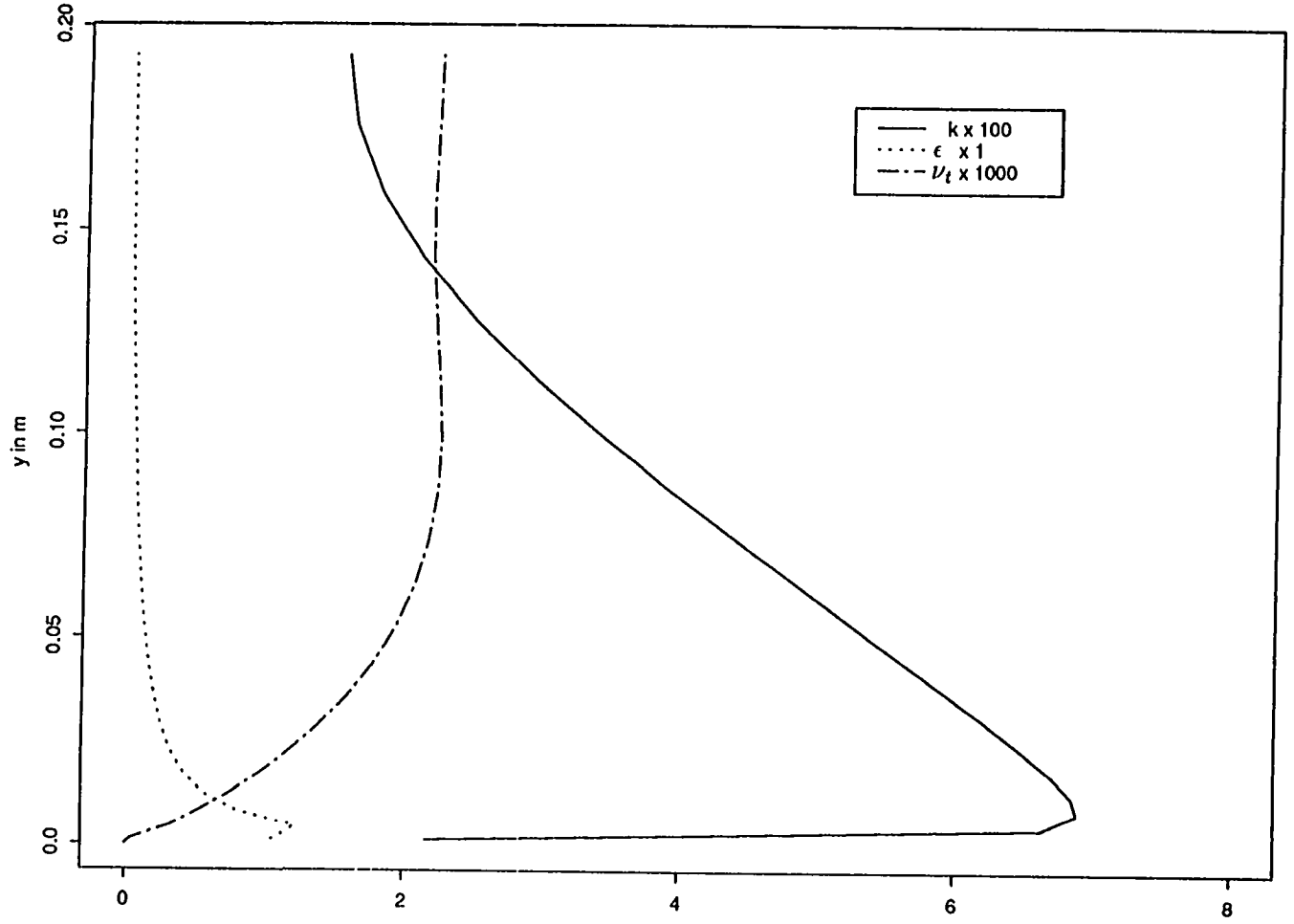

Figure 7.9: Vertical Profiles of k,ϵ and ν_t.

in nature the ripples that form are of much shorter wavelength. However numerical experiments would need to be performed to ascertain this fact.

7.4 Hydraulic Jump Simulation

Hydraulic jump is formed when the supercritical flow changes to subcritical flow. This normally happens when the flow enters in a supercritical state and encounters obstacles or downstream control. In our model problem flow enters in a supercritical state. The flow height is specified at the downstream end. Due to this hydraulic jump is formed. The operating conditions are a little different from the one we had earlier. We had to do this to compare our results with the experimental data presented by Gharangik(1991). The experimental conditions of Gharangik(1991) are :

$$Fr_{in} = 6.65 \quad , \quad Re_{in} = 0.078 \times 10^6, \theta = 0.0, L = 14.0m \text{ and} H_{in} = 2.4cm. \quad (7.4)$$

In fig.7.10 the effect of mesh spacing on hydraulic jump is shown. It can be seen that the computed height of the free surface is slightly lower that the measured profile and also the location of the jump does not match very well with that presented by Gharangik(1991). It is difficult to determine the cause. But it must be remarked that the experimental conditions such as wall roughness, inlet velocity and turbulence profiles are not known and these could have some effect on the numerical simulation results.

In Figs.7.11 and 7.12 the effects of wall roughness and channel inclination are shown. Here again the results agree qualitatively with physical intuition but will need to be verified quantitatively if complete confidence on the flow model is to be gained. In Fig.7.13 the time evolution of the hydraulic jump is shown. The steady state stream line patterns are shown in Fig.7.14. Small zone of recirculation can be observed just behind the jump. This has also been observed by Rahman(1991).

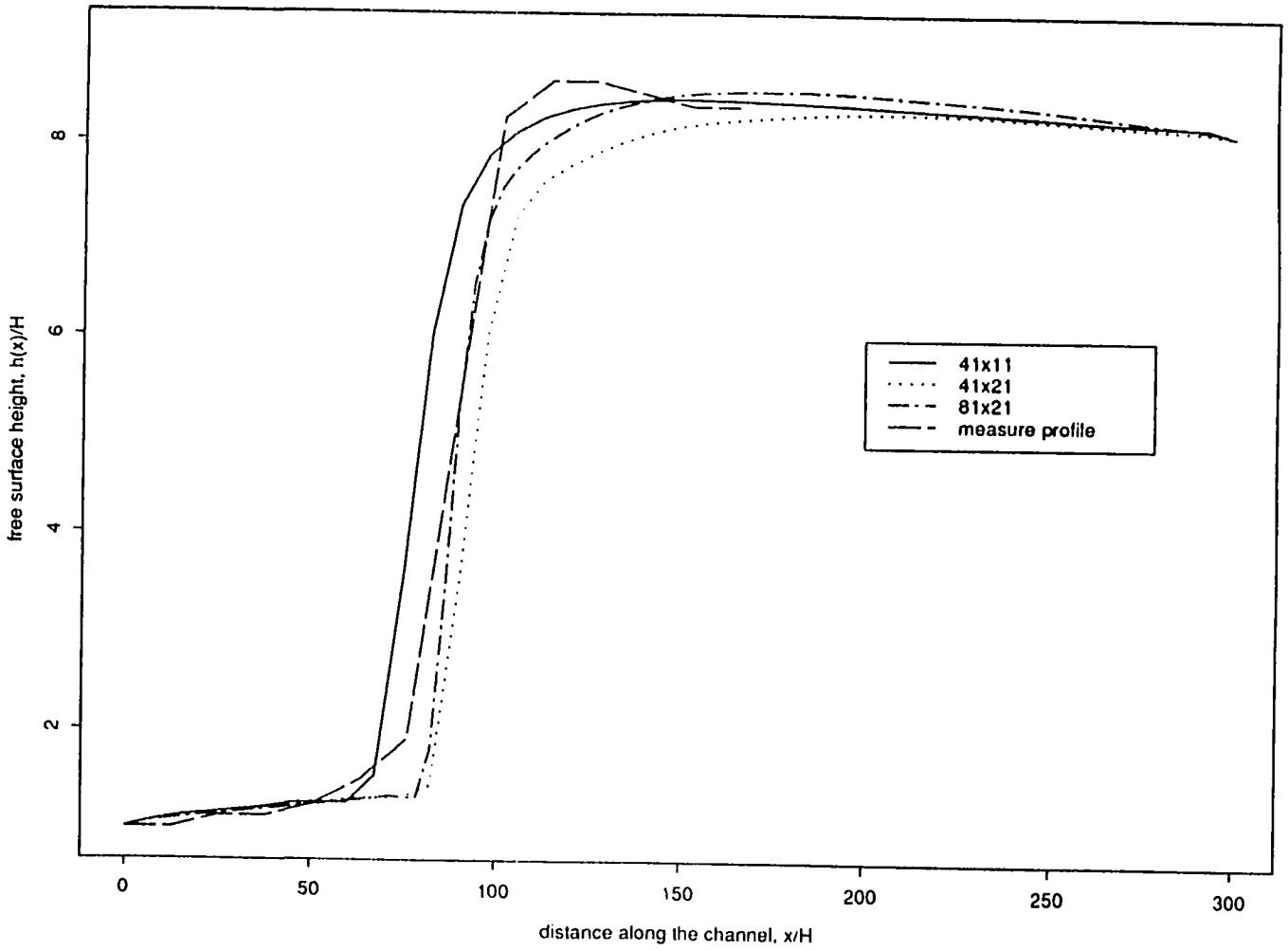

Figure 7.10: Effect of mesh spacing on hydraulic jump profile

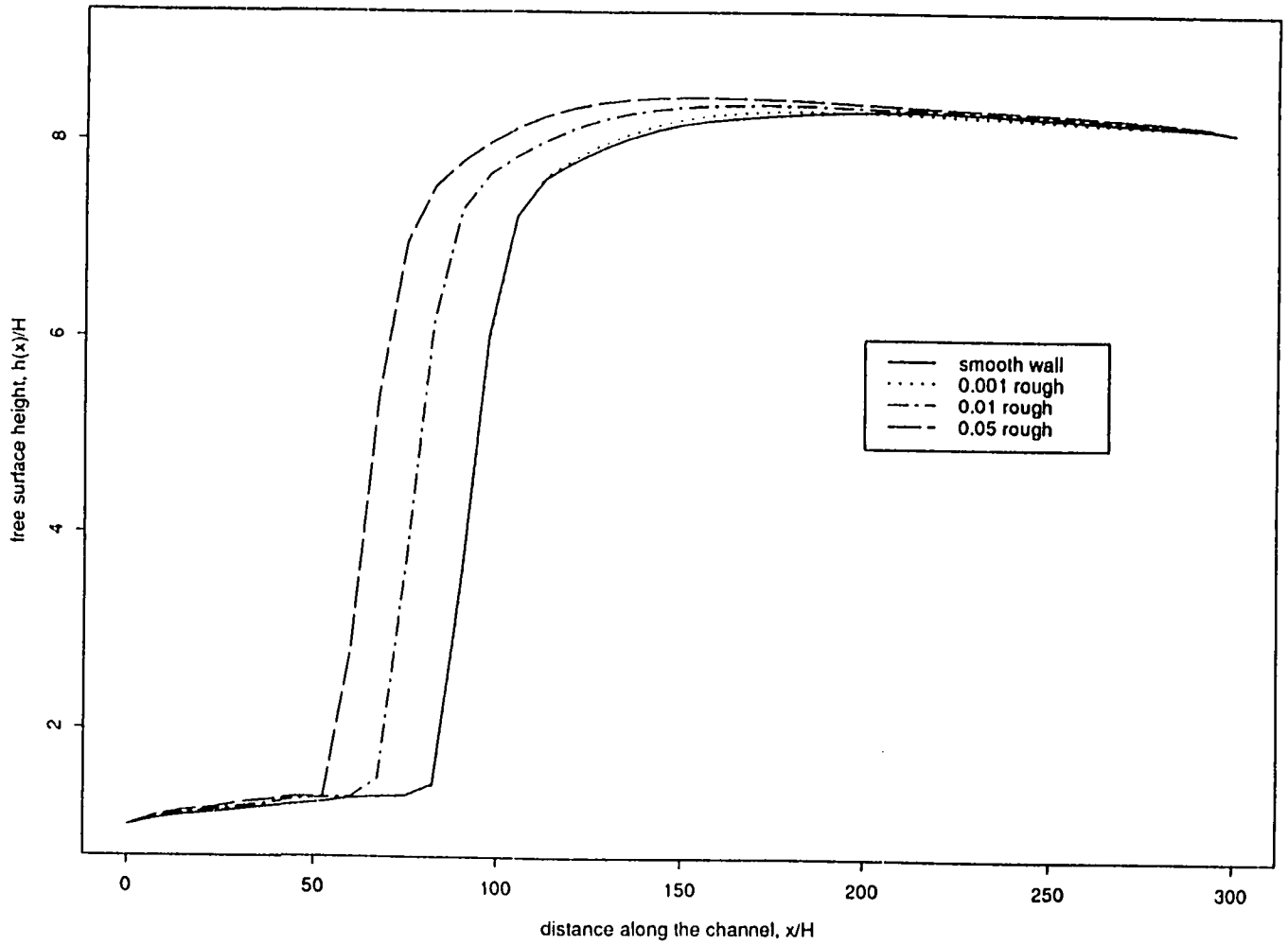

Figure 7.11: Effect of wall roughness on hydraulic jump profile

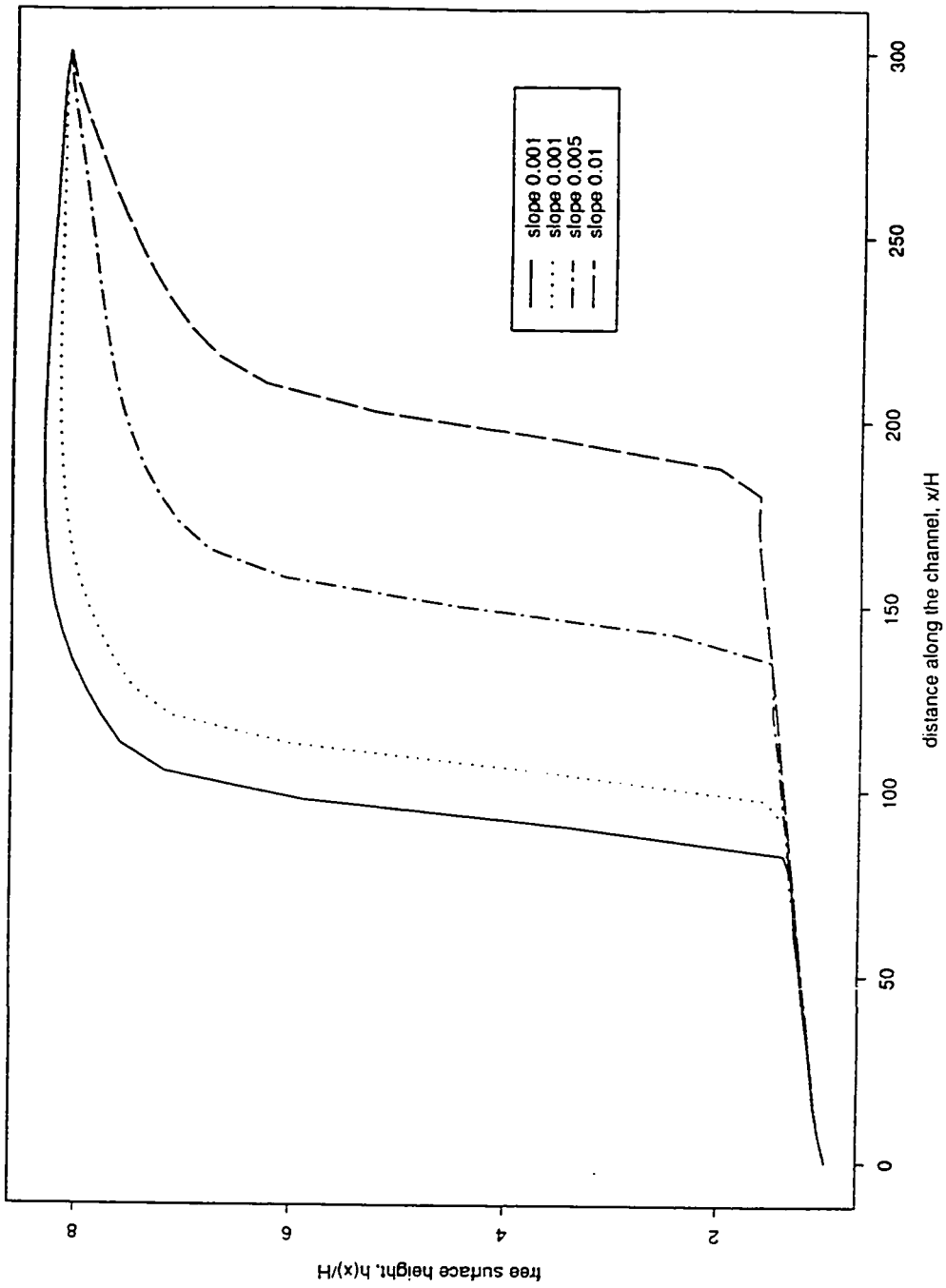

Figure 7.12: Effect of inclination on hydraulic jump profile

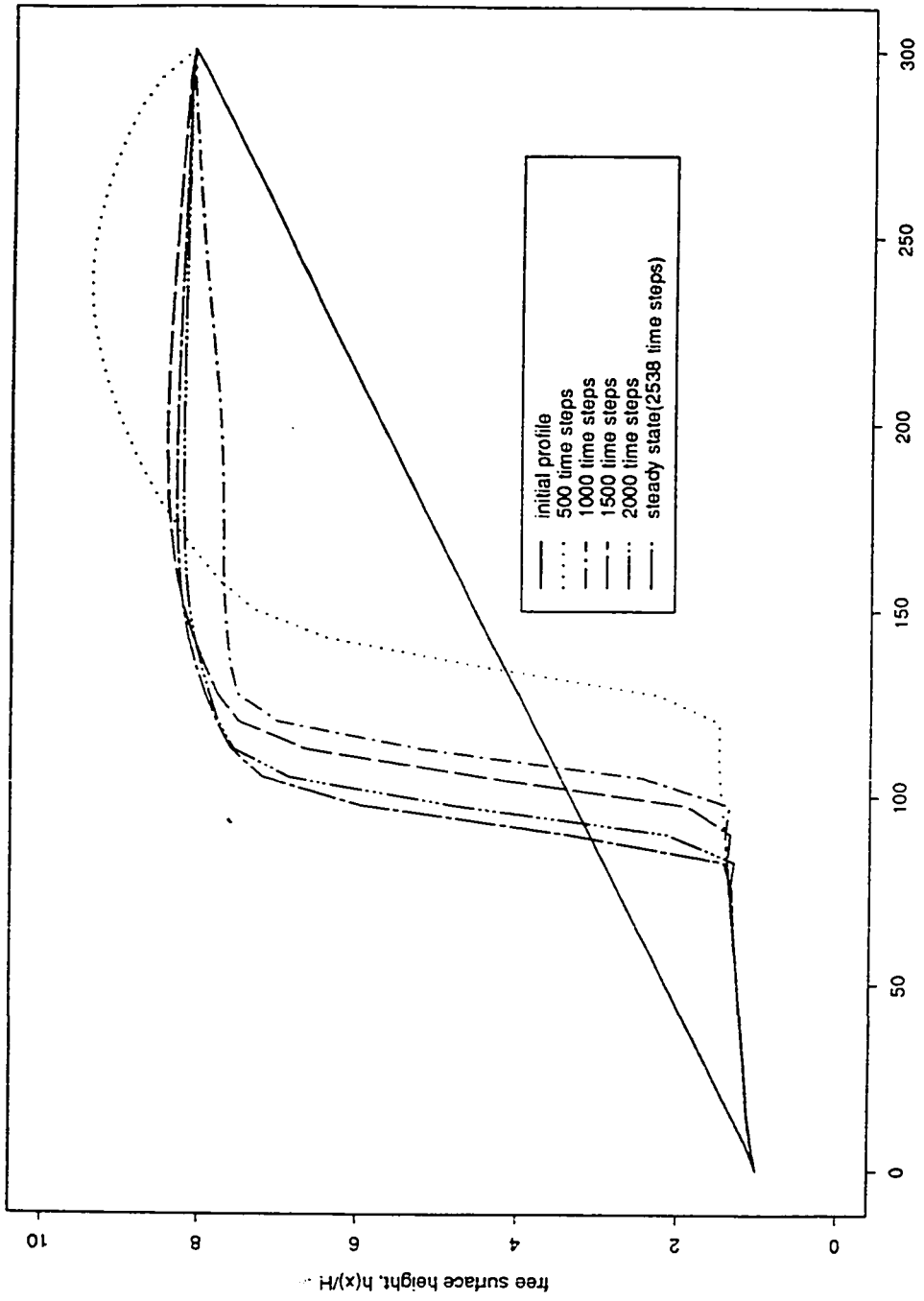

Figure 7.13: Time evolution of free surface

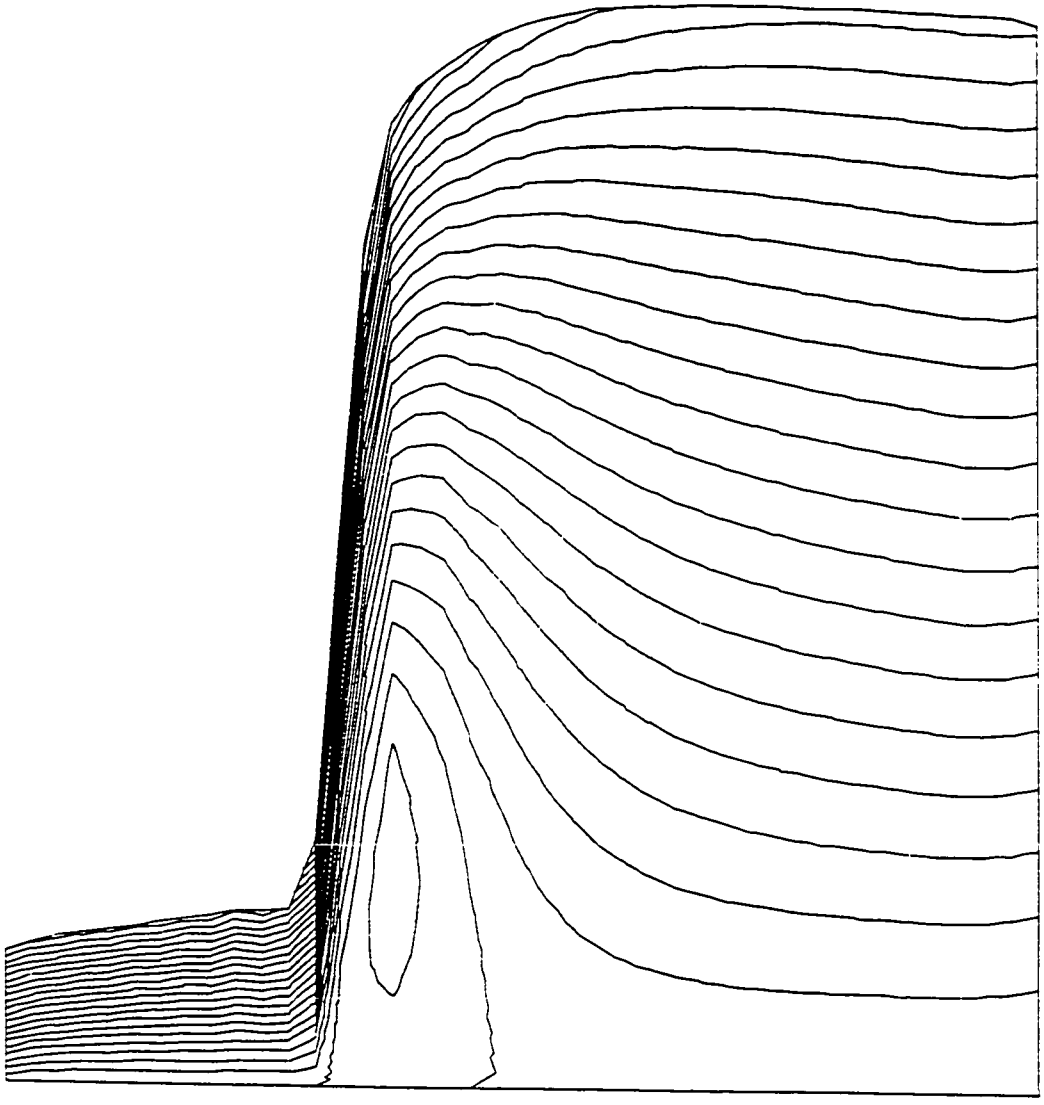

Figure 7.14: Stream line patterns

Chapter 8

SEDIMENT TRANSPORT MODELING

Water flowing in natural channels often has the ability to scour sand, gravel, or even large boulders from the bed or banks and sweep them downstream. This phenomenon is termed sediment transport. Sediment material can be *cohesive* or *noncohesive.* In cohesive sediments there are adhesive forces between particles, e.g, clayey sands or soils. In noncohesive sediment transport there are no adhesive forces between particles. Only noncohesive sediments have been considered for our research. The basic mechanism responsible for sediment motion is the drag force exerted by the fluid flow on individual grains.

Usually, three modes of particle motion are distinguished:

- Rolling and sliding motion or both;
- saltation motion; and
- suspended particle motion.

When the value of the bed-shear velocity just exceeds the critical value for initiation of motion, the particles will be rolling and sliding or both, in continuous contact with the bed. For increasing values of the bed-shear velocity, the particles will be moving along the bed by more or less regular jumps, which are called saltations. When the value of the bed-shear velocity exceeds the fall velocity of the particles, the sediment particles can be lifted to a level at which the upward turbulent forces will be comparable with or of higher order than the submerged weight of the particles and

as a result the particles may go in suspension. Usually, the transport of particles by rolling, sliding and saltating is called bed-load transport.

8.1 The Threshold of Sediment Movement

As the velocity of the flow is steadily increased the shear stress exerted by the fluid on the bed increases and at a particular value the sediment particles begin to move. This is called the *threshold* condition. The most commonly used expression to derive the critical shear stress for initiation of sediment motion is that derived by Shields [Naden, 1988]. In this simple model, shown in Fig.8.1, the threshold of sediment motion is defined in terms of the dimensionless bed shear stress $(\tau_c/(\rho_s - \rho)gD$ where τ_c is critical shear stress, ρ_s is the density of sediment, ρ is the density of water, g is the acceleration due to gravity, and D is particle diameter). This is plotted against the grain Reynolds number ($Re_* = u_*D/\nu = f(D/\delta)$ where u_* is the bed shear velocity, ν is the kinematic viscosity of water, δ is the depth of laminar sublayer) which is a measure of the type of flow boundary. Under smooth boundary conditions ($Re_* < 2$), the particles are enclosed in laminar film and their motion is independent of turbulence. As Reynolds number increases, there is a zone of transition as the laminar film begins to break up, while for rough boundary conditions ($Re_* > 400$), the critical dimensionless bed shear stress becomes constant.

In addition to the problem of the initiation of movement, it is important to know how much sediment moves. As already mentioned moving sediment can be classified either as bedload or suspended load and is depicted in Fig.8.2. The predominant mode of transport depends on the size, shape, and density of particles in respect to the velocity and turbulence field of the water body. Bedload transport is mainly dependent on the shear stress at the bed whereas the suspended load is affected by the complete velocity profile.

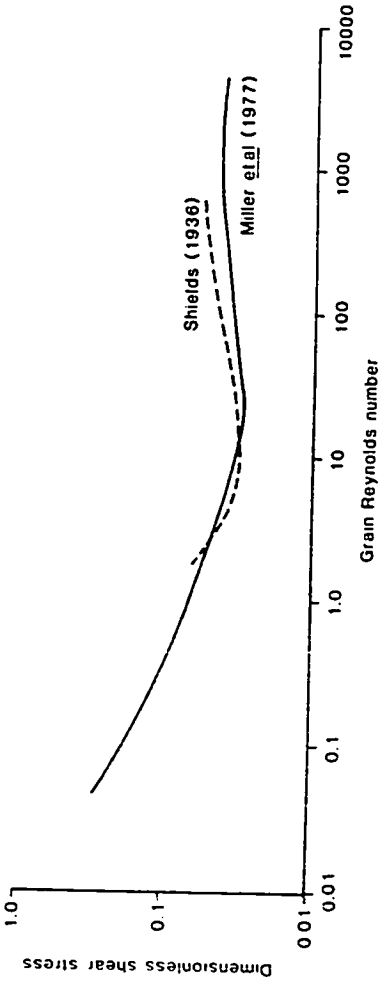

Figure 8.1: Shields Criterion for Initiation of Motion

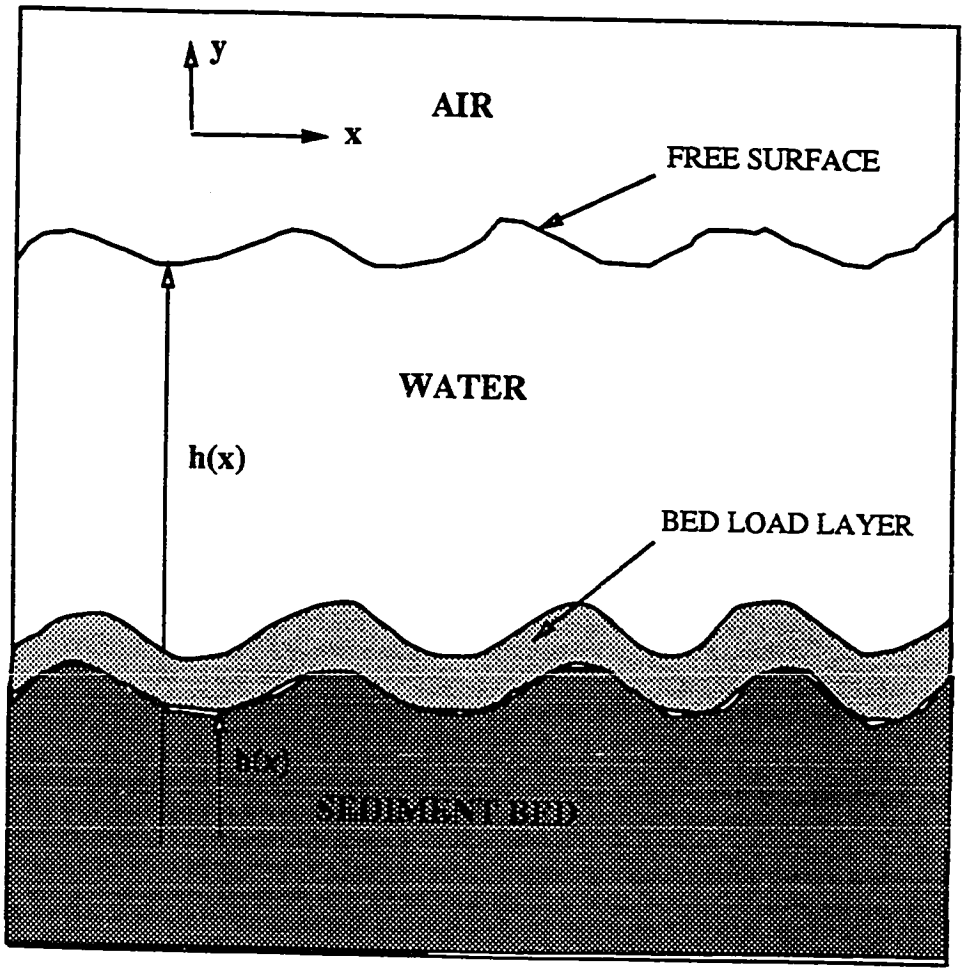

Figure 8.2: Sediment transport model

8.2 Suspended Load

After the threshold of motion has been passed, and sediment movement is well established, some of the sediment will be carried in the form of suspended load; in the case of strong flows and fine sediment, the amount of suspended load may be substantial. This material is maintained in suspension by the action of turbulence. Due to turbulence not only momentum transfer but also mixing of scalar properties such as temperature, color, salt concentration, sediment concentration etc. take place across adjacent fluid layers. Thus in a turbulent flowing fluid of kinematic eddy viscosity ν_t carrying sediment of volume concentration c, the volumetric rate of sediment transfer across the stream lines, per unit area, in the direction of positive y is equal to

$$-\nu_t \frac{dc}{dy} \tag{8.1}$$

The sediment particle fall downward due to their weight at a speed w_s called the fall velocity of the sediment particles. Thus the downward flux of sediment due to gravity is given by cw_s. If the suspended load is in equilibrium then the downward flux due to gravity equals the upward flux due to fluid turbulence and we have

$$cw_s + \nu_t \frac{\partial c}{\partial y} = 0 \tag{8.2}$$

Assuming a parabolic distribution for the eddy viscosity based on Prandtl's mixing length theory and a logarithmic law behaviour for the velocity above eqn.8.2 can be integrated in the vertical direction.

$$\frac{c}{c_a} = \left[\frac{a(h-y)}{y(h-a)}\right]^{w_s/\kappa u_*} \tag{8.3}$$

where c_a is the concentration at a height a above the bed. Since there is no way of knowing c_a initially, above eqn. 8.3 cannot give absolute values of the concentration, but can only give their relationship to the unknown c_a. What this means is that the total load cannot be predicted by the above theory; to do this it is necessary to know something of the mechanism of entrainment at the bed.

The nonequilibrium suspended sediment transport is usually determined by an advection-diffusion transport equation for sediment concentration.

$$\frac{\partial c}{\partial t} + u\frac{\partial c}{\partial x} + (v - w_s)\frac{\partial c}{\partial y} = \frac{\partial}{\partial x}(\nu_t \frac{\partial c}{\partial x}) + \frac{\partial}{\partial y}(\nu_t \frac{\partial c}{\partial y}) \tag{8.4}$$

This would be the equation we would be solving to obtain suspended sediment concentration.

8.3 Bed Load

The vertical turbulent fluctuations are suppressed close to the bed. There is therefore no turbulent transfer term, $\nu_t \frac{\partial c}{\partial y}$, to balance the sediment fall term cw_s. Upward movement of sediment across the bedload plane is supplied by the mechanism of entrainment. Thus the difference between deposition (cw_s) and entrainment determines whether sediment moves from bedload into suspended load or vice versa.

Determining the bedload transport is very difficult and the problem is compounded by the statistical nature of the problem of entrainment. Many bed load formulas have been developed, some purely empirical, others having a back ground of semirational and semidimensional arguments. The reader is referred to Henderson(1966) for some important bed load formulas. The one we are going to use is that given by van Rijn(1984a) and is stated in the next section.

8.4 Sediment Modeling Issues

The mechanism of sediment transport is not very well understood and there are many issues which are still being researched. Some of the features which make sediment transport so difficult to understand and predict are:

- Wide variation in sizes and shapes of sediment.
- The effect sediment has on the fluid turbulence is not known.

- Sediment does have some effect on the pressure distribution.
- It is not clear if the eddy viscosity of sediment is the same as the eddy viscosity of momentum.
- Clearly the particle fall velocity in a turbulent particle laden flow would be different from that in a quiescent clear liquid.
- entrainment at the bed is a stochastic process.

8.5 Sediment Model Chosen

In this section the sediment transport model chosen by us is discussed. This model has been proposed by van Rijn(1884a, 1984b, 1984c).

1. Compute the Shields critical bed-shear velocity, $u_{*,cr}$.

$$\begin{aligned} D_* \leq 4, &\quad \Theta_{cr} = 0.024(D_*)^{-1} \\ 4 < D_* \leq 10, &\quad \Theta_{cr} = 0.014(D_*)^{-0.64} \\ 10 < D_* \leq 20, &\quad \Theta_{cr} = 0.04(D_*)^{-0.10} \\ 20 < D_* \leq 150, &\quad \Theta_{cr} = 0.013(D_*)^{0.29} \\ D_* > 150, &\quad \Theta_{cr} = 0.055 \end{aligned} \tag{8.5}$$

   where $\Theta_{cr} = \frac{u_{*,cr}^2}{(s-1)gD_{50}}$.

2. The three characteristic parameters that determine the sediment transport are calculated as:

$$D_* = D_{50}\left[\frac{(s-1)g}{\nu^2}\right]^{1/3} \tag{8.6}$$

$$T = \frac{u_*^2 - u_{*,cr}^2}{u_{*,cr}^2} \tag{8.7}$$

$$Z = \frac{w_s}{\beta \kappa u_*} \tag{8.8}$$

where D_* is called the particle parameter, T, the transport parameter and Z, the suspension parameter. D_{50} is the 50th percentile sediment particle size, s is the specific density; g is the acceleration of gravity; ν is the kinematic viscosity; u_* is the shear stress at the bed determined from the flow code; $u_{*,cr}$ is the critical bed-shear velocity for bed movement given by Shields, κ = von-Karman constant.

3. Compute reference level, a

$$a = 0.5\Delta, \text{ or} k_s, \text{ with}(a_{min} = 0.01h), \tag{8.9}$$

where Δ is the bed-form height.

4. Compute reference concentration, c_a

$$c_a = 0.015 \frac{D_{50}}{a} \frac{T^{1.5}}{D_*^{0.3}} \tag{8.10}$$

5. Compute particle size of suspended sediment, D_s

$$\frac{D_s}{D_{50}} = 1 + 0.011(\sigma_s - 1)(T - 25) \tag{8.11}$$

where σ_s is the standard deviation of the particle size.

6. Compute fall velocity, w_s

$$\begin{aligned} D_s < 100\mu m, &\qquad w_s = \tfrac{1}{18} \tfrac{(s-1)gD_*^2}{\nu} \\ 100\mu m \le D_s < 1000\mu m, &\qquad w_s = 10 \tfrac{\nu}{D_s} \left[1 + \tfrac{0.01(s-1)gD_*^3}{\nu^2}\right]^{0.5} - 1 \\ D_s > 1000\mu m, &\qquad w_s = 1.1\left[(s-1)gD_s\right]^{0.5} \end{aligned} \tag{8.12}$$

The fall velocity calculated from the above equation is corrected for the effect sediment concentration has on the fall velocity of a particle using the expression, $w_{s,m} = (1-c)^4 w_s$.

7. Compute suspended load from the transport eqn.

$$\frac{\partial c}{\partial t} + u\frac{\partial c}{\partial x} + (v - w_s)\frac{\partial c}{\partial y} = \frac{\partial}{\partial x}(\nu_t \frac{\partial c}{\partial x}) + \frac{\partial}{\partial y}(\nu_t \frac{\partial c}{\partial y}) \tag{8.13}$$

8. Compute total suspended load from

$$S_s = \int_{b+a}^{h} ucdz \tag{8.14}$$

9. Bed load transport is computed from

$$S_b = 0.053\,[(s-1)g]^{0.5}\, D_{50}^{1.5} \frac{T^{2.1}}{D_*^{0.3}} \tag{8.15}$$

The bed deformation is computed from the continuity equation for the sediment concentration.

$$\frac{\partial b}{\partial t} + \frac{1}{1-\phi}\left[\frac{\partial S_s}{\partial x} + \frac{\partial S_b}{\partial x}\right] = 0 \tag{8.16}$$

where S_s and S_b are the total suspended load and bedload flux respectively, and ϕ is the porosity of the bed.

Chapter 9

RESULTS AND DISCUSSION : SEDIMENT TRANSPORT SIMULATION

With the sediment transport model outlined in the previous chapter we tried to simulate sedimentation and bed deformation. The time scales associated with hydrodynamics and bed movement are different by orders of magnitude. Usually the flow reaches steady state in a matter of seconds whereas the channel bed deformation takes place over days or months in hydraulic engineering situations and over hundreds of years in geomorphological situations. Hence generally the steady state solution of the fluid flow is determined first and this computed flow field is used to study bed deformation. The logical structure of determining sediment transport is shown in the form of a flow chart in Fig.9.1. The calculations are stopped when the channel bed reaches equilibrium (no change in channel bed with time) or quasi-equilibrium (bed forms migrate along the channel bed). The flow model developed previously is combined with the sediment transport model described in the previous section.

A test problem involving bed erosion and deposition is studied and the channel bed and free surface locations over different times are shown in Figs.9.2-9.9. Some of the qualitative aspects of the simulation seem to be correct. For instance over dunes the free surface height reduces in the case of sub-critical flow and this is shown correctly in our simulations. However, it must be admitted that the simulations need to be run for a much longer time than what has been shown. Since our aim was only to get an idea about the workings of the sediment transport code we did not proceed further.

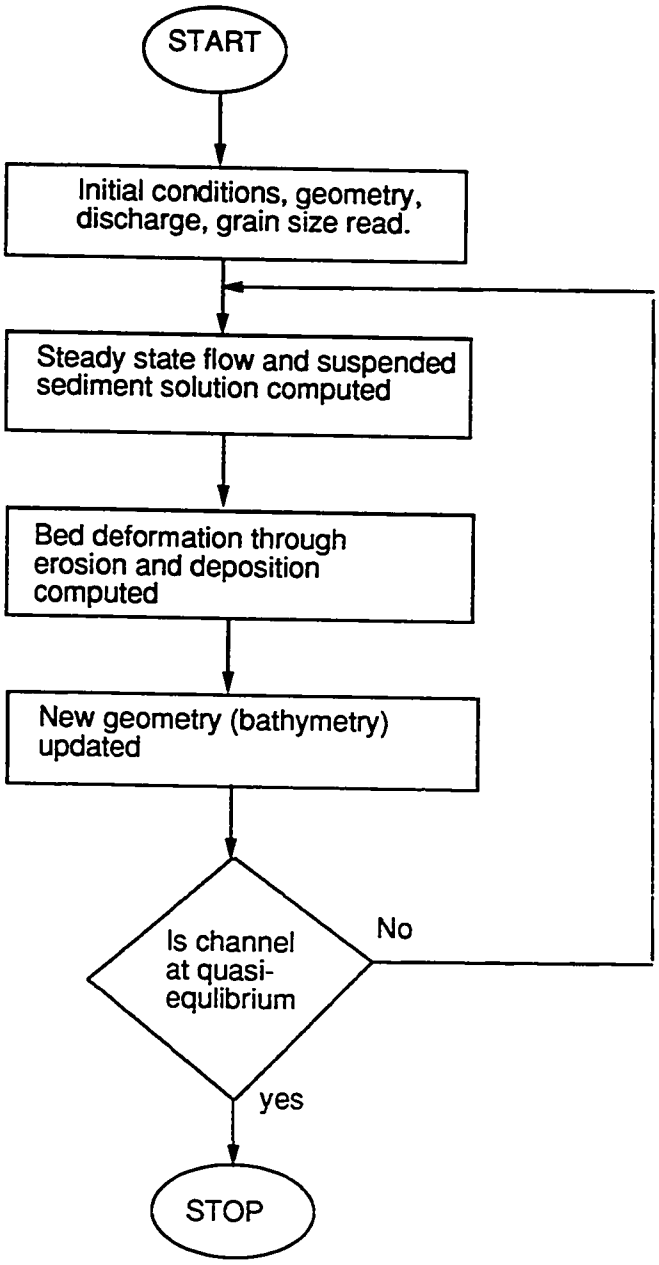

Figure 9.1: Sediment transport model problem

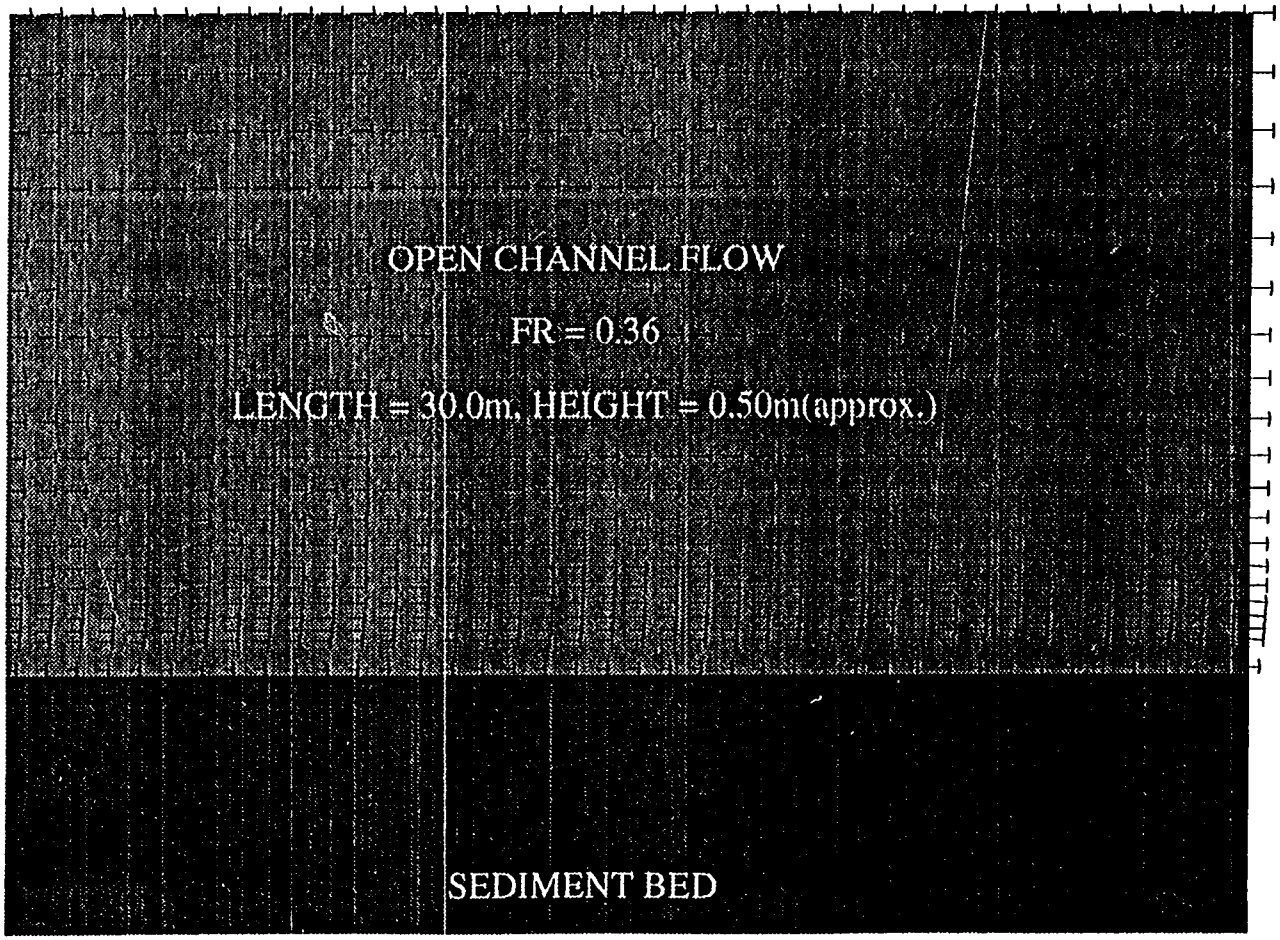

Figure 9.2: Sediment bed and free surface at time, t=0.0 hrs

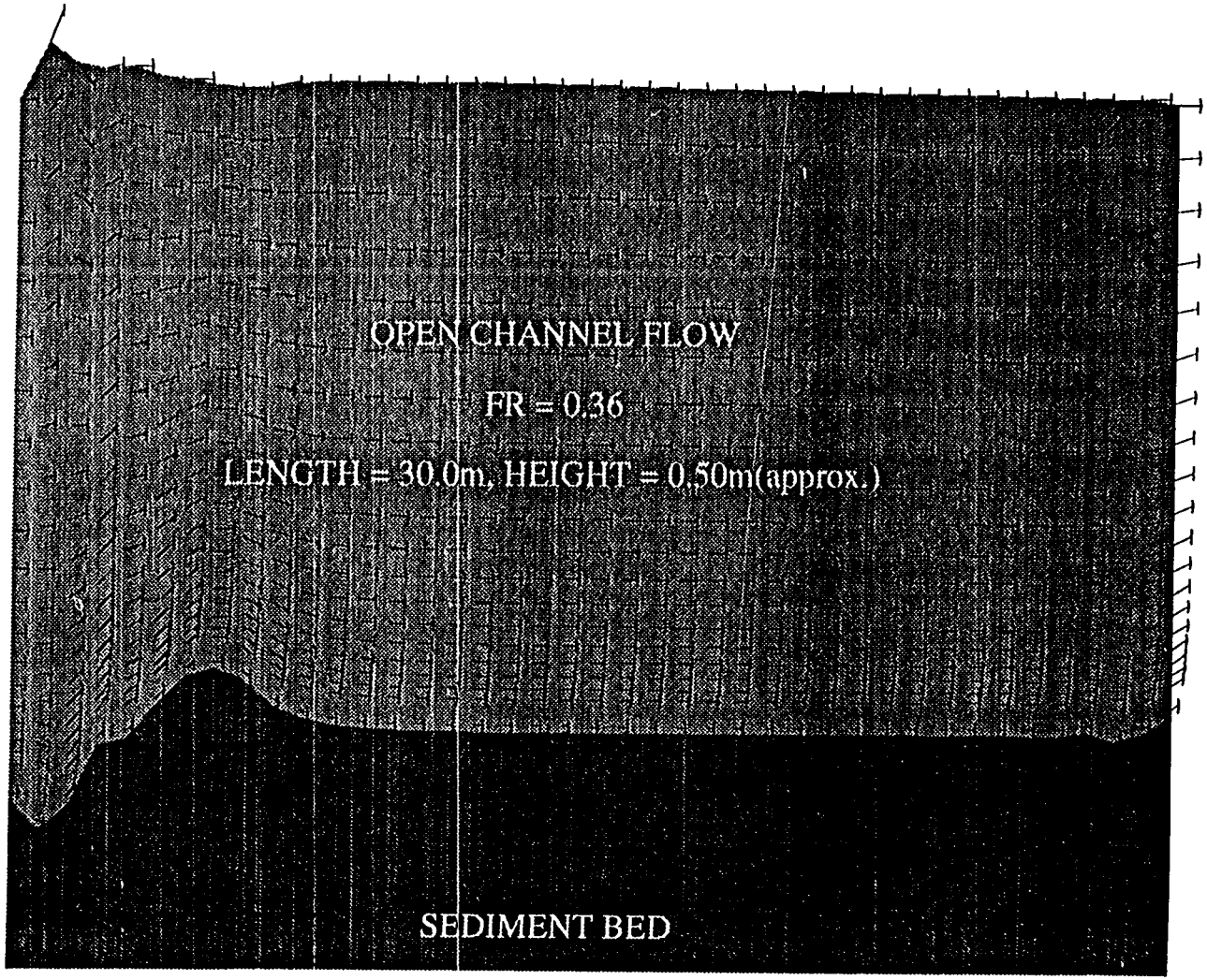

Figure 9.3: Sediment bed and free surface at time, t=1.3 hrs

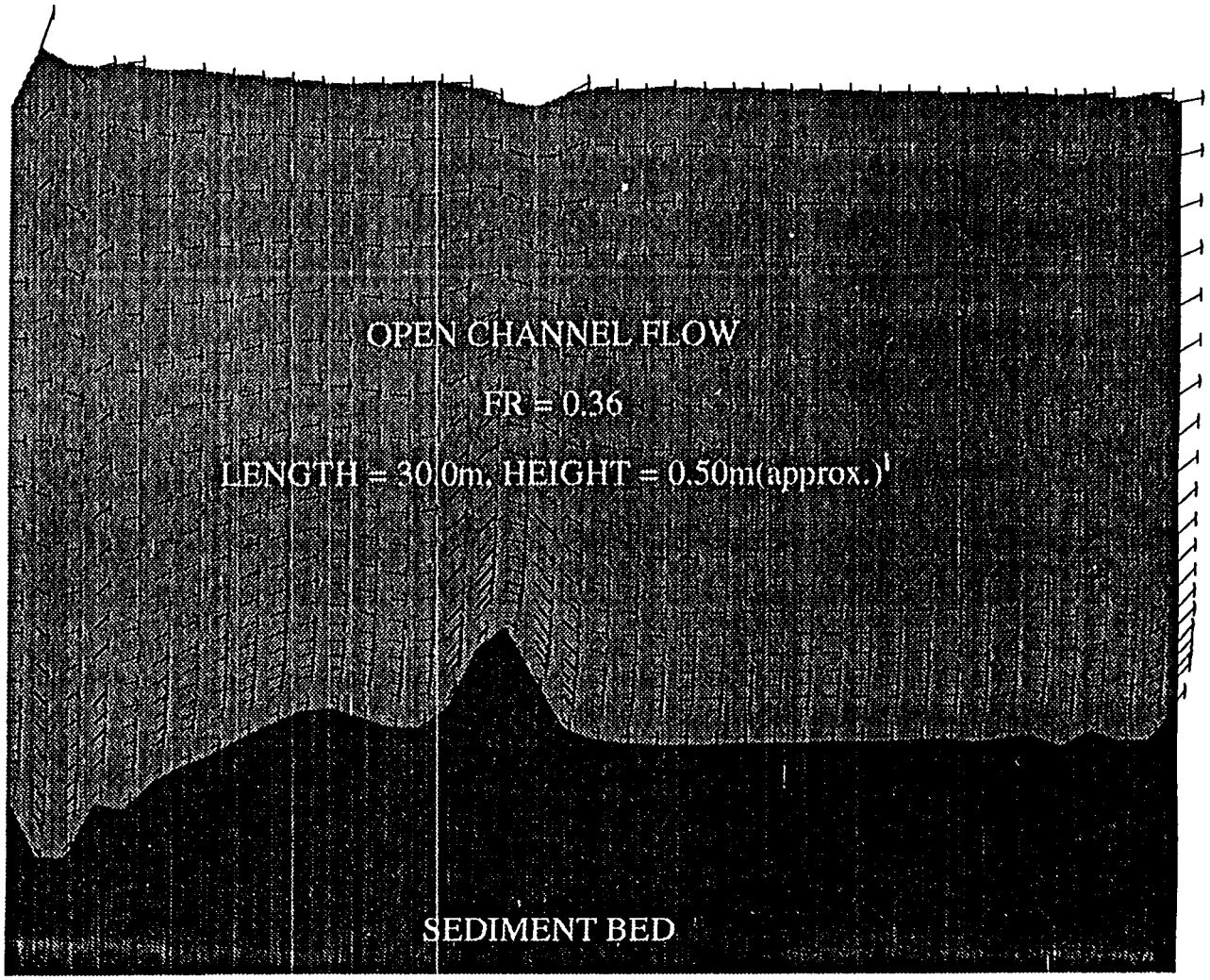

Figure 9.4: Sediment bed and free surface at time, t=3.2 hrs

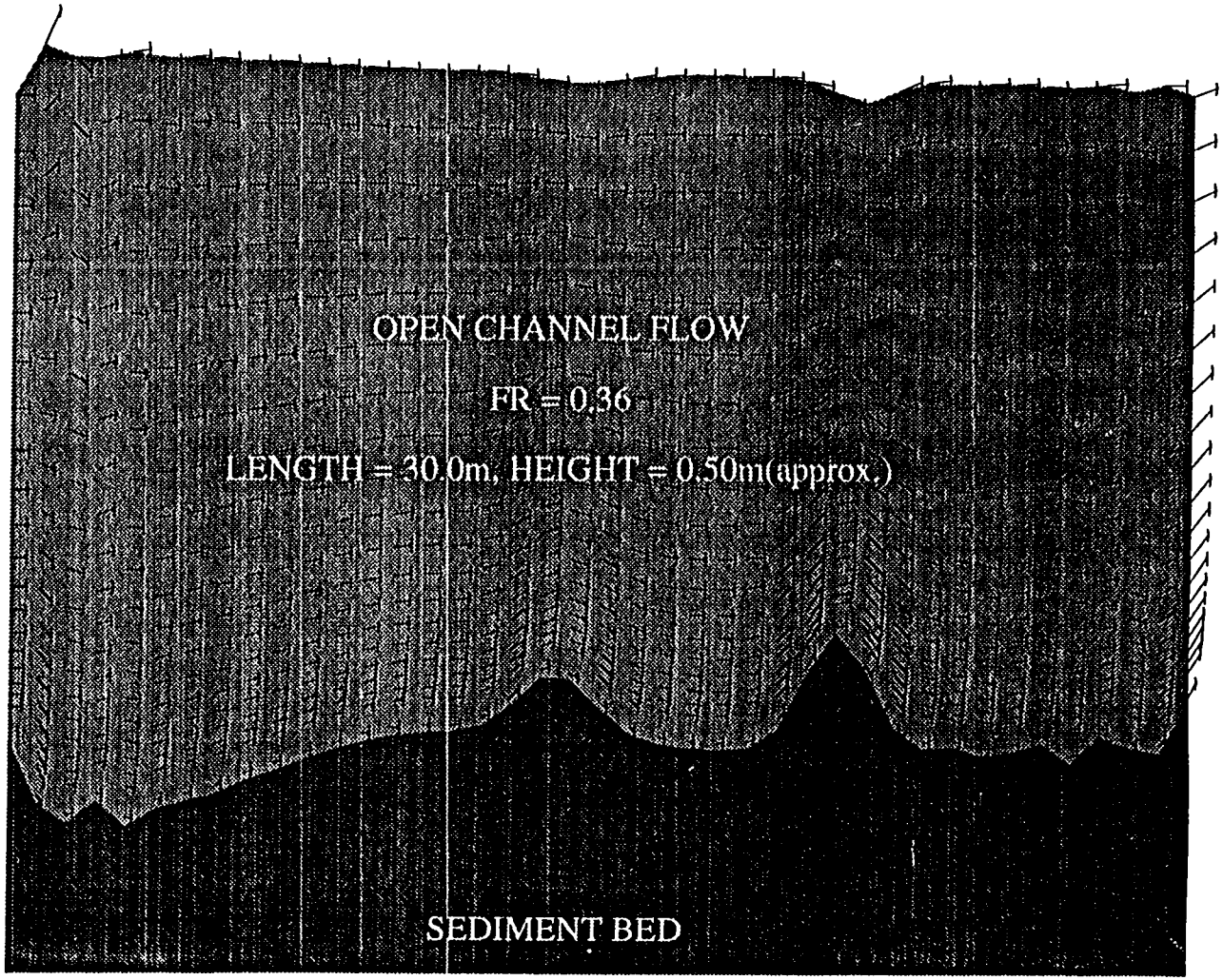

Figure 9.5: Sediment bed and free surface at time, t=5.5 hrs

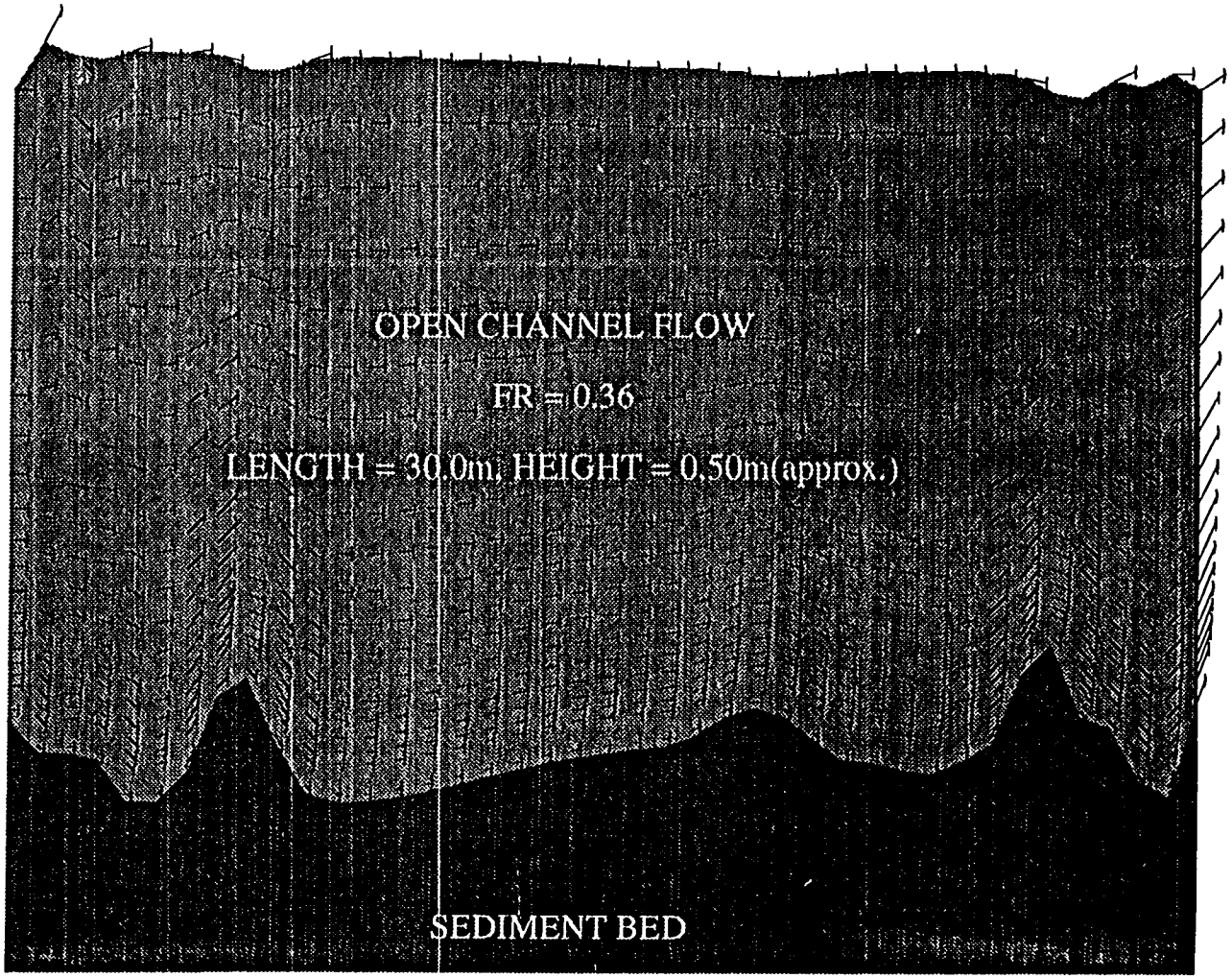

Figure 9.6: Sediment bed and free surface at time, t=9.9 hrs

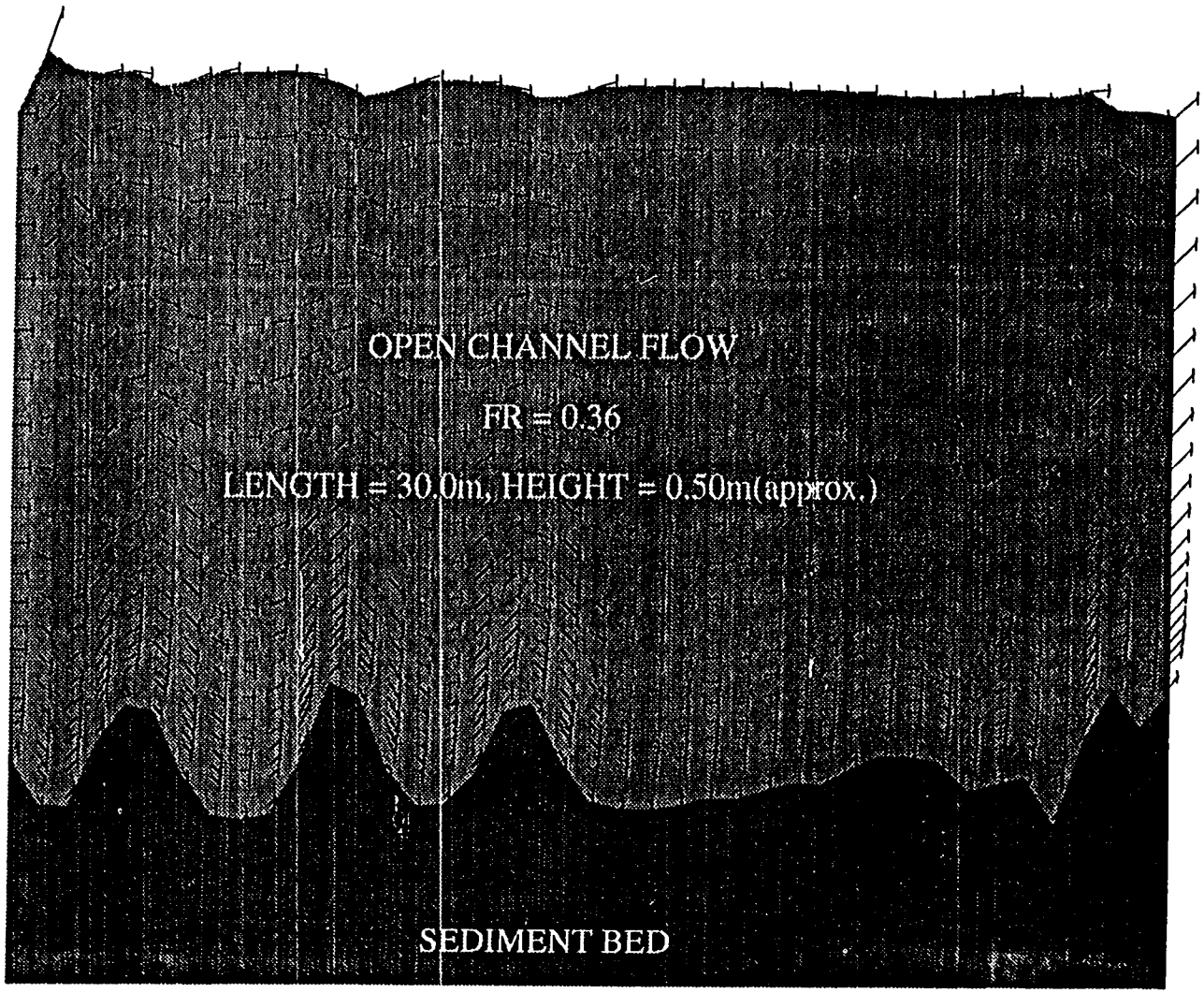

Figure 9.7: Sediment bed and free surface at time, t=14.3 hrs

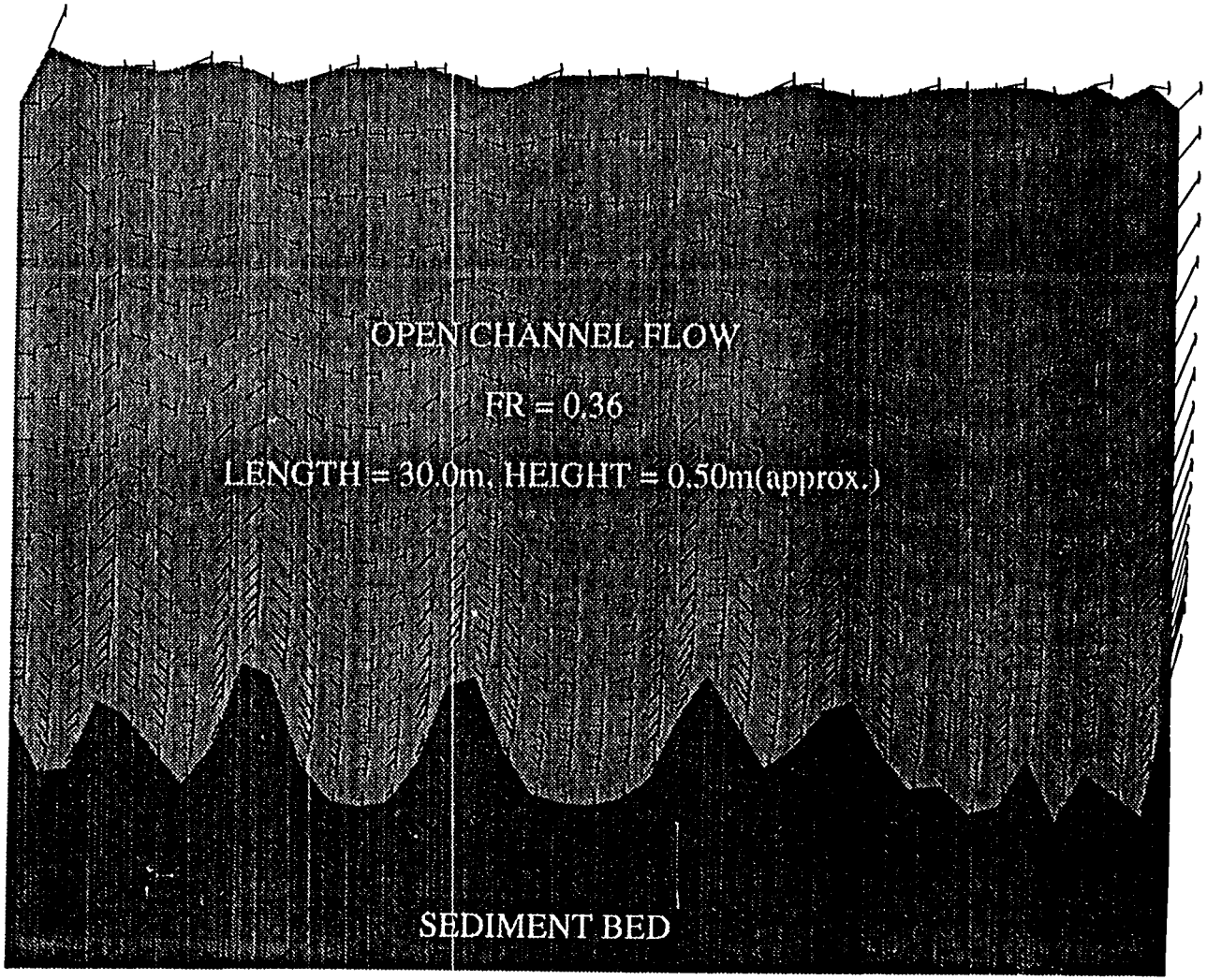

Figure 9.8: Sediment bed and free surface at time, t=19.4 hrs

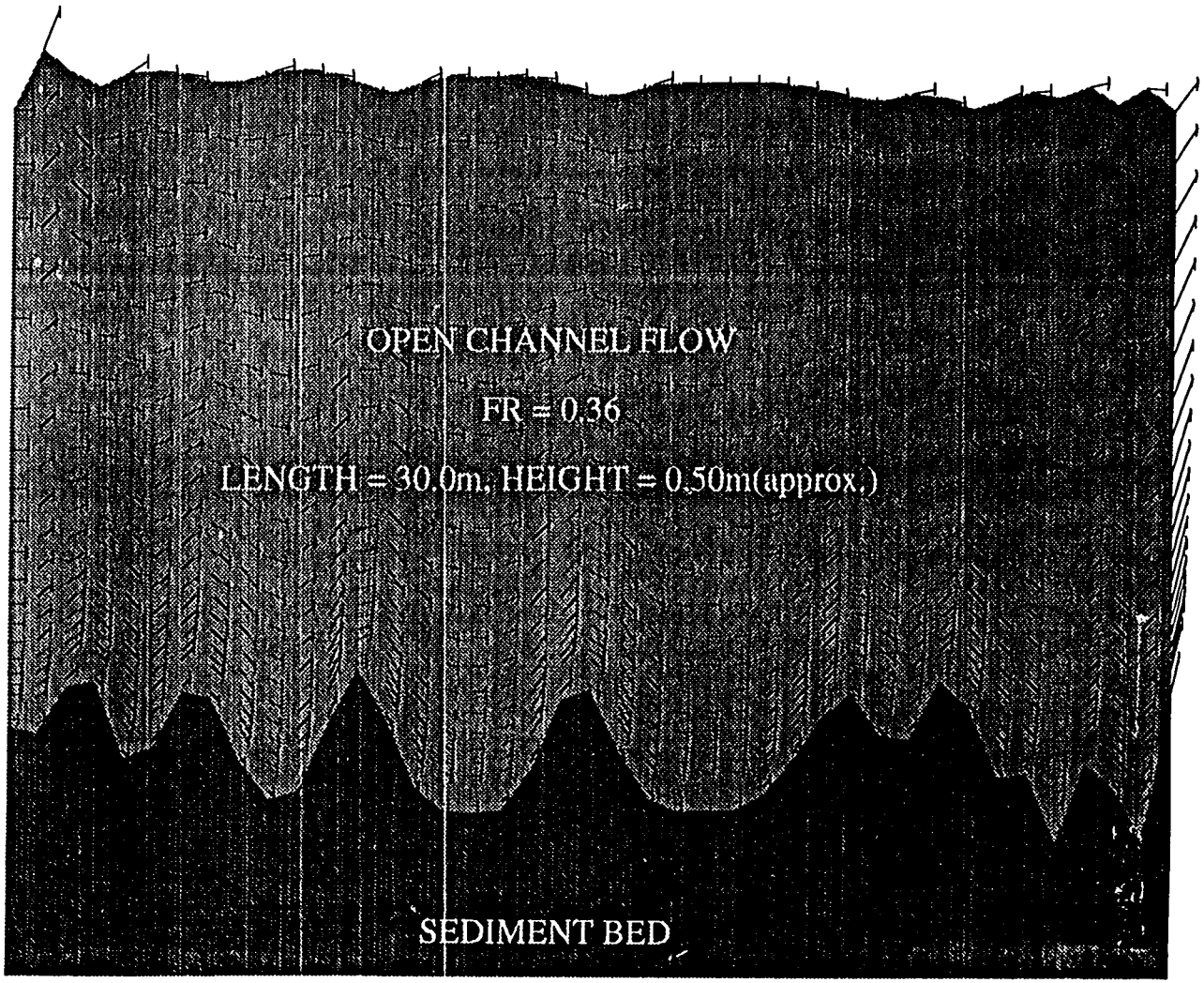

Figure 9.9: Sediment bed and free surface at time, t=21.1 hrs

Chapter 10

GENERAL CONCLUSIONS

10.1 Conclusion

It may be useful to turn back to the chapter on open channel flow where we outlined the various capabilities our code need to have to successfully simulate open channel flow and sedimentation. Some of the features of this research are stated her again:

1. 2-D Reynolds averaged equations have been solved without any depth averaging.
2. The problem posed by the changing free surface has been overcome using the ALE approach.
3. Eddy viscosity is determine using $k - \epsilon$ model.
4. Time marching is done through projection scheme and spatial discretization is done with the help of 3-noded triangles and Galerkin finite element formulation.
5. It has been established that the procedure has the ability to handle high gradient situations such as hydraulic jump.
6. The code determines the suspended sediment using an advection-diffusion transport equation and bedload through empirical relationships. The procedure is simple and can quite easily be modified to include any new developments in sediment mechanics.
7. It has been proved that the code does have the ability to predict the evolution of bed form features such as dunes and anti-dunes.

10.2 Future Work

Our ultimate goal is to develop complete 3-D flow and sediment transport model. As a next step in achieving this objective we plan to parallelize the code. This parallelized code would then be used to study some real life large scale problems. After complete confidence is achieved on the 2-D code attempts would be made to develop a 3-D procedure.

We recognize the fact that what has been achieved is very small compared what needs to be done. We believe that a beginning has been made in the right direction and with the tremendous progress being made in computer hardware and algorithms our dream of developing a full 3-D procedure is realizable.

Bibliography

[1] Anderson, D. A., Tannehill, J. C. and Pletcher, R. H., *Computational Fluid Mechanics and Heat Transfer*, p.247, McGraw-Hill Book Co., (1984).

[2] ASCE Task Committee on Turbulence Models in Hydraulic Computations, "Turbulence Modeling of Surface Water Flow and Transport," *J. of Hyd. Engg.*, **114**, pp.970-1073, part:1-5, (1988).

[3] Baker, A. J., "Finite Element Solution Algorithm for Viscous Incompressible Fluid Dynamics," *Int. J. Num. Methods Engg.*, **6**, pp.89-101, (1973).

[4] Brooks, A. N. and Hughes, T. J. R., "Streamline Upwind/Petrov-Galerkin Formulations for Convection Dominated Flows with Particular Emphasis on the Incompressible Navier-Stokes Equations," *Comp. Meth. Appl. Mech. Engg.*, **32**, pp.199-259, (1982).

[5] Celik, I. and Rodi, W., "Simulation of Free Surface Effects in Turbulent Channel Flows," *PhysicoChemical Hydrodynamics*, **5**, pp.217-227, (1984).

[6] Chorin, A. J., "A Numerical Method for Solving Viscous Incompressible Flow Problems," *J. Comput. Phys.*, **2**, pp.12-26, (1967).

[7] Chorin, A. J., "Numerical Solution of the Navier-Stokes Equations," *math. Comp.*, **22**, pp.745-762, (1968).

[8] Cheng, R. T., "Numerical Solution of the Navier-Stokes Equations by the Finite Element Method," *Phys. Fluids*, **15**, pp.2098-2105, (1972).

[9] Chow, V. T., *Open-Channel Hydraulics*, McGraw Hill Book Co., (1959).

[10] Ferziger, J. H., "Simulation of Incompressible Turbulent Flows," *Jl. of Computational Physics*, **69**, pp.1-48, (1987).

[11] FIDAP Users Manual, Revison 6.0, Fluid Dynamics International, Inc., (1991).

[12] Gharangik, A. M. and Chaudhary, M. H., "Numerical Simulation of Hydraulic Jump," *J. Hyd. Engg.*, **117**, pp.1195-1211, (1991).

[13] Gresho, P. M. and Sani, R. L., "On Pressure Boundary Conditions for the Incompressible Navier-Stokes Equations," *Int. J. Num. Meth. Fluids*, **7**, p.1111, (1987).

[14] Harlow, F. H. and Welch, J.E., "Numerical Calculation of Time-Dependent Viscous Incompressible Flow of Fluid with Free Surface," *Phys. Fluids*, **8**, pp.2182-2189, (1965).

[15] Henderson, F. M., *Open Channel Flow*, Macmillan, (1966).

[16] Hinze, J. O., *Turbulence*, McGraw Hill Book Co., (1975).

[17] Hirsch, C., *Numerical Computation of Internal and External Flows*, John Wiley & Sons, (1988).

[18] Hirt, C. W., Cook, J. L. and Butler, T. D., "A Lagrangian Method for Calculating the Dynamics of an Incompressible Fluid with Free Surface," J. Comput. Phys., **5**, pp.103-124, (1970).

[19] Hirt, C. W., Amsden, A. A., and Cook, J. L., "An Arbitrary Lagrangian-Eulerian Computing Method for All Flow Speeds," *J. Comput. Phys.*, **14**, pp.227-253, (1974).

[20] Huebner, K. H., The Finite Element Method for Engineers, 2nd Edn., John Wiley & Sons, (1982).

[21] Iga, M., and Reddy, J. N., "Penalty Finite Element Analysis of Free Surface Flows of Power-Law Fluids," *Int. J. Non-Linear Mechanics*, **24**, pp.383-399, (1989).

[22] Jobson, H. E., "Vertical Transfer in Open Channel Flow," *J. Hyd. Div.*, Proc. ASCE, pp.703-724, (1970).

[23] Kawahara, M. and Miwa, T., "Finite Element Analysis of Wave Motion," *Int. J. Num. Methods Engg.*, **20**, pp.1193-1210, (1984).

[24] Lai, Chintu., "Numerical Modelling of Unsteady Open-channel Flow," *Advances in Hydroscience*, **14**, pp.161-333.

[25] Launder, B. E. and Spalding. D. B., "The Numerical Compuation of Turbulent Flows," *Comput. Meth. Appl. Mech. Engg.*, **3**, 269-289, (1974).

[26] McCarty, T. A., Wang, S. Y., Su, T. Y. and Hu, K. K., "A Multishape Function Finite Element Model for Three Dimensional Flow Simulation," *Third Intl. Symp. on River Sedimentation*, Univ. of Mississippi, pp.1594-1601, (1986).

[27] Miller, M. C., McCave, I. N. and Komar, P. D., "Threshold of Sediment Under Unidirectional Currents," *Sedimentology*, **24**, pp.507-527, (1977).

[28] Naden, P. S., "Models of Sediment Transport in Natural Streams," *Modeling Geomorphological Systems*(ed. M. G. Anderson), pp.217-258, (1988).

[29] Nallasamy, M., "Turbulence Models and Their Applications to the Prediction of Internal Flows: A Review," *Comp. Fluids*, **15**, pp.151-194, (1987).

[30] Rahman, M. M., Faghri, A. and Hankey, W. L., "Computation of turbulent flow in a thin layer of fluid involving a hydraulic jump," *J. Fluids Engg.*, **113**, pp.411-418, (1991).

[31] Ramaswamy, B. and Kawahara, M., "Lagrangian Finite Element Analysis Applied to Viscous Free Surface Fluid Flow," *Int. J. Num. Methods Fluids*, **7**, pp.953-984, (1987).

[32] Ramaswamy, B., "Numerical Simulation of Unsteady Viscous Free Surface Flow," *J. of Comput. Phys.*, **90**, pp.396-430, (1990).

[33] Rodi, W., *Turbulence Models and Their Applications in Hydraulics – A State of the Art Review*, 2nd Edn. International Association for Hydraulic Research, Delft (1984).

[34] Saito, H. and Scriven, L. E., "Study of Coating Flow by the Finite Element Method," *J. of Comput. Phys.*, **42**, pp.53-76, (1981).

[35] Sarma, K. V. N. and Syamal, P., "Supercritical Flow in Smooth Open Channels," *J. Hyd. Engg.*, **117**, pp.54-63, (1991).

[36] Shen, J., "On Error Estimates of Projection Methods for Navier-Stokes Equations: First-Order Schemes," *SIAM J. Numer. Anal.*, **29**, pp.57-77, (1992).

[37] Sheng, Y. P., Lick, W., Gedney, R. T. and Molls, F.B., "Numerical Computation of Three-Dimensional Circulation in Lake Erie: A Comparison of a Free-surface Model and Rigid-lid Model," *J. of Oceanography*, pp.713-727, (1978).

[38] Sotiropoulos, F. and Abdallah, S., "The Discrete Continuity Equation in Primitive Variable Solutions of Incompressible Flow," *J. Comput. Phys.*, **95**, pp.212-227, (1991).

[39] Su, T. Y., Trujillo, J., Yue, J. P. and Wang, S. Y., "Multilevel Finite Element Simulation of Sediment Transport in Mobile bay," *Proc. Third Int. Symp. on River Sedimentation*(ed. Wang etal), Univ. of Mississipi, pp.323-328, (1986).

[40] van Rijn, L. C., "Sediment Transport, Part 1: Bed Load Transport," *J. of Hyd. Engg.*, **110**, pp.1431-1456, (1984a).

[41] van Rijn, L. C., "Sediment Transport, Part 2: Suspended Load Transport," *J. of Hyd. Engg.*, **110**, pp.1613-1642, (1984b).

[42] van Rijn, L. C., "Sediment Transport, Part 3: Bed Forms and Alluvial Roughness," *J. of Hyd. Engg.*, **110**, pp.1733-1753, (1984c).

[43] Zienkiewicz, O. C. and Wu, J., "Incompressibility Without Tears - How to Avoid Restrictions of Mixed Formulation," *Private Communication.*